CONFIDENTIAL

Copy 332
RM E51G26

NACA RM E51G26

E51G26

TECH LIBRARY KAFB, NM
0143254

6691

RESEARCH MEMORANDUM

EFFECT OF ANGLE OF ATTACK AND EXIT NOZZLE DESIGN ON THE PERFORMANCE OF A 16-INCH RAM JET AT MACH NUMBERS FROM 1.5 TO 2.0

By Eugene Perchonok, Fred Wilcox, and Donald Pennington

Lewis Flight Propulsion Laboratory
Cleveland, Ohio

CLASSIFIED DOCUMENT

This document contains classified information affecting the National Defense of the United States within the meaning of the Espionage Act, USC 50:31 and 32. Its transmission or the revelation of its contents in any manner to an unauthorized person is prohibited by law.
Information so classified may be imparted only to persons in the military and naval services of the United States, appropriate civilian officers and employees of the Federal Government who have a legitimate interest therein, and to United States citizens of known loyalty and discretion who of necessity must be informed thereof.

NATIONAL ADVISORY COMMITTEE
FOR AERONAUTICS

WASHINGTON
October 5, 1951

CONFIDENTIAL

319.98/13

TECH LIBRARY KAFB, NM
0143254

2254

NATIONAL ADVISORY COMMITTEE FOR AERONAUTICS

RESEARCH MEMORANDUM

EFFECT OF ANGLE OF ATTACK AND EXIT NOZZLE DESIGN ON THE PERFORMANCE OF A 16-INCH RAM JET AT MACH NUMBERS FROM 1.5 TO 2.0

By Eugene Perchonok, Fred Wilcox, and Donald Pennington

SUMMARY

An investigation of the performance of a 16-inch ram jet engine having a single oblique-shock all-external compression inlet designed for a flight Mach number of 1.8, was conducted in the NACA Lewis 8- by 6-foot supersonic wind tunnel. Data were obtained at Mach numbers from 1.5 to 2.0 and angles of attack from 0° to 10°. Three exit nozzles were used; a cylindrical extension of the combustion chamber, a 4° half-angle converging nozzle with a 0.71 contraction ratio, and a converging-diverging nozzle having a 0.71 contraction ratio plus re-expansion to essentially major body diameter.

Operation at angle of attack of 10° caused a reduction in combustion efficiency of about 10 percentage points from the value obtained at 0° angle of attack and also caused reductions in diffuser pressure recovery and air mass flow. At a given combustion-chamber total-temperature ratio, there was a small decrement of the thrust component in the flight direction and a large increase in the thrust component in the lift direction as the angle of attack was increased from 0° to 10°.

With the burner configuration employed, the cold-flow subcritical diffuser pulsations were damped to very low amplitudes by burning. Also, there was some evidence that the external engine body drag with the converging exit nozzle decreased below the cold-flow value as the exhaust-gas temperature was raised.

Maximum engine efficiencies were obtained with the converging-diverging exit-nozzle configuration. Graphite served as a satisfactory material for this nozzle.

PERMANENT RECORD

[redacted]

INTRODUCTION

An experimental investigation of the performance of a 16-inch ram jet engine was conducted in the NACA Lewis laboratory 8- by 6-foot supersonic wind tunnel. The engine, which had a single oblique-shock all-external compression inlet was designed for a flight Mach number of 1.8. Engine performance with a constant-area exit nozzle at 0° angle of attack is presented in reference 1. Data are now available at angles of attack from 0° to 10° and with two additional exit-nozzle configurations, a conical converging nozzle and a converging-diverging nozzle.

2254

Effects of angle of attack on internal engine performance and a comparison of operation and performance for the three different exit-nozzle configurations are presented and discussed. The subcritical diffuser flow stability under both cold-flow and burning conditions is also evaluated. Data are presented at Mach numbers from 1.5 to 2.0 and for Reynolds numbers (based on engine length) from 77.5 to 81.1×10^{6}.

The converging-diverging nozzle insert was fabricated of graphite, and its durability and wear under typical operating conditions are discussed.

APPARATUS

The engine and burner configuration and the tunnel installation were the same as described in reference 1. A schematic diagram of the engine is shown in figure 1 and a detailed tabulation of engine coordinates is given in table I. Also indicated in figure 1 are details of the static and total-pressure surveys at stations 2 and x. The inlet was designed so that at a stream Mach number M_0 of 1.8 the shock generated by the 50° conical spike would fall slightly ahead of the cowl lip. The combustion chamber was 16 inches in diameter.

Three exit-nozzle configurations were investigated, a constant area nozzle, a converging nozzle, and a converging-diverging nozzle. The over-all engine length from spike tip to nozzle exit was the same for all three configurations, 16 feet. The converging nozzle was conical with a convergence half angle of 4° and a ratio of exit area to combustion-chamber area of 0.71. The converging-diverging nozzle also had a ratio of throat area to combustion chamber area of 0.71 and then re-expanded to essentially combustion chamber diameter. This nozzle consisted of a graphite insert and its contour and retaining details are indicated in figure 2.

A schematic diagram of the flame holder, fuel manifold, and spray nozzle arrangement is given in figure 3. The flame-holder surface open area was 133 percent of the combustion-chamber frontal area. Propylene

2254

oxide was used as fuel. The vortex-type pilot burner was operated with a blend of 50-percent gasoline and 50-percent propylene oxide by volume.

An independently supported water-cooled tail rake was used to measure the exit momentum at angles of attack of 0° and 6° for all but the graphite nozzle. Static wall orifices were located along the fore section of the diffuser outer shell and along the diffuser inner wall and center body. Fluctuations in pressure loads on the outer shell and internally at the diffuser exit were determined with commercial differential-pressure pickups.

The total temperature and pressure in the test section depended on the stream Mach number as well as atmospheric conditions and could not be independently controlled.

SYMBOLS

The following symbols are used in this report:

A	area (sq ft)
A_{max}	area on which all coefficients are based (area of 16 in. diameter circle)
C	force coefficient, $\frac{F}{q_0 A_{max}}$
(C_t-C_d)	propulsive thrust coefficient
C_p	static pressure coefficient, $\frac{p-p_0}{q_0}$
F	force (lb)
F_t	net internal thrust (lb)
$\frac{(F_t-F_d)V_0}{\eta_b h W_f J}$	reduced engine efficiency (percent)
f/a	fuel-air ratio
h	lower heating value of fuel (13,075 Btu/lb for propylene oxide)
J	mechanical equivalent of heat (778 Btu/ft lb)

M	Mach number
m	mass flow (slugs/sec)
m/m_0	mass flow ratio, ratio of the actual air mass flow through engine to the mass flow contained in free-stream tube having a diameter equal to diffuser-inlet diameter
P	total pressure (lb/sq ft absolute)
p	static pressure (lb/sq ft absolute)
$\frac{\Delta p}{p}$	amplitude coefficient, $\frac{\text{maximum pressure - minimum pressure}}{\text{average pressure}}$
q	dynamic pressure $\left(\frac{\gamma}{2}\right) p M^2$
r	radius (in.)
t	static temperature, $^{\circ}F$
V	velocity (ft/sec)
W_f	fuel flow (lb/sec)
α	angle of attack (deg)
γ	ratio of specific heats
η_b	combustion efficiency
τ	total-temperature ratio across engine

Subscripts:

a	air entering engine
d	total external body drag
H	component of net thrust in flight direction
j	jet thrust
t	net internal thrust
V	component of net thrust in lift direction

2254

2254

x air flow measuring station (59 in. from cowl lip)

0 free stream

1 engine inlet

2 alternate air flow measuring station (18 in. from cowl lip)

3 combustion chamber inlet

4 nozzle inlet

6 nozzle exit

PROCEDURE

A cold-flow investigation similar to that of reference 1 was made with the converging nozzle to determine the effect on external body drag of boattailing the exit nozzle. As in reference 1, a dummy strut was employed to separate external body drag from the total drag measured by the tunnel balance. The flame holder was removed and a remotely adjustable valve inserted at the combustion chamber inlet to vary the diffuser exit Mach number over both the subcritical and supercritical flow ranges.

The mass air flow through the engine reported herein was computed from pressure data obtained at station x (see fig. 1) and on the basis of additional independent air flow measurements is considered accurate to ± 3 percent. The diffuser pressure recovery is also based on pressures measured at this station because at 0° angle of attack the total pressure at station 3, the combustion chamber inlet, was found to be the same as that at station x within the accuracy of the measurement. The burner-inlet Mach numbers M_3 are based on the annular area at the diffuser exit, station 3.

Jet thrusts for the cold-flow investigation were determined from the measured air flow, two static wall orifices at the nozzle exit, and a total-pressure rake located just inside of the nozzle exit. With combustion, the constant-area and converging nozzles were assumed choked at the exit and the jet thrust was computed from the tail-rake total-pressure data. For angles of attack greater than 6° however, the water-cooled tail rake could not be used and other means were required to obtain the exit total pressure. For each exit configuration the same relation was determined to exist between M_3 and the ratio of nozzle exit total pressure to total pressure at station x P_6/P_x for both 0° and 6° angle of attack. This same relation between M_3 and P_6/P_x was assumed at 10°, and P_6 could then be determined from the values of M_3 and P_x.

The water-cooled tail rake was not used during tests with the converging-diverging exit nozzle. Since the choking cross-sectional areas for both the convergent and the convergent-divergent nozzles were equal, the flow through the divergent section of the latter nozzle was assumed to be isentropic, and the convergent nozzle data was then used to evaluate the exit gas temperature for the convergent-divergent nozzle. The net propulsive thrust was determined by adding the support strut drag to the balance reading and the net internal thrust obtained by adding the propulsive thrust value to the total cold-flow external body drag.

2254

The combustion efficiency, defined as the ratio of the change in energy of the gases flowing through the engine to the lower heating value of the fuel injected, and all other internal engine performance parameters were computed by the methods generally employed and outlined in references 2 and 3. Neither the combustion efficiency nor the total-temperature ratio across the engine were corrected for cooling losses.

The quantities computed from pressure instrumentation were assumed to represent a valid time average of the actual value during pulsing operation (see reference 4).

RESULTS AND DISCUSSION

Effect of Angle of Attack

Diffuser pressure recovery. - Subcritical and supercritical diffuser performance data are presented in figure 4 for M_0 values of 1.5, 1.8, and 2.0 and angles of attack of 0°, 6°, and 10° for both cold-flow and burning conditions. No measurable effect of burning on diffuser total-pressure recovery was observed. Both the diffuser pressure recovery and the air mass flow decreased as the angle of attack was progressively increased from 0° to 10°. For the Mach numbers investigated, the reduction in mass flow was between 3 and 4 percent. In general, the sensitivity of pressure recovery and air mass flow to changes in angle of attack increased both with angle of attack and M_0. These results are consistent with previously published data (reference 5).

The effect of angle of attack on the critical M_3 is not readily predictable, for it depends not only on the decrease in air flow but on the drop in critical pressure recovery as well. For a pressure loss amounting to several percent, $M_0 = 1.8$ and 2.0, the critical M_3 increased slightly as the angle of attack was raised. At $M_0 = 1.5$ the pressure loss was little more than 1 percent and the critical M_3 was reduced because of a decrease in air flow.

2254

Diffuser pulsing. - Subcritical diffuser instability was observed at M_0 of 1.8 and 2.0. This instability causes periodic fluctuations in the diffuser static and total pressures. The frequency of these pulses is the same throughout the diffuser, but the amplitude depends on the location at which the measurement is made. As a typical example of the effect of operating condition on such fluctuations, the cold-flow frequency and amplitude variation of the static pressure at the diffuser exit are presented for 0° angle of attack in figure 5. The amplitude of the fluctuation is expressed in coefficient form as $\frac{\Delta p}{p}$ where Δp is the difference between the average maximum and the average minimum pressures and p is the mean pressure at the point of measurement.

For the two cases illustrated, pulsing was first encountered near the critical M_3 value, and once initiated the amplitude of the pulse increased sharply as M_3 was lowered. At an M_3 of approximately 0.11, amplitude coefficients of the order of 0.8 (representing pressure fluctuations of ± 7.4 lb/sq in.) were observed. Further reductions of M_3 resulted in a reversal in trend and a drop in amplitude. Although it is not too well defined by these data, there is also a trend toward reduced amplitudes as M_0 is lowered. Little change in amplitude was obtained when the angle of attack was changed from 0° to 6° but when it was increased from 6° to 10°, the cold-flow amplitudes were reduced considerably.

Once pulsing was established, the frequencies at both $M_0 = 1.8$ and 2.0 were essentially similar. This result is consistent with the theory of reference 6 and is due primarily to similarly shaped pressure recovery curves at both Mach numbers. A theoretical frequency curve, based on the theory of reference 6, is shown for $M_0 = 2.0$ and good agreement with experiment is observed from the inception of pulsing to $M_3 = 0.15$. Although below this value the trends between theory and experiment are similar, experimental frequencies up to 3 cycles per second higher than predicted were observed.

The combined effect of inserting a flame holder and burning on frequency and amplitude, both on the cowl and internally at the diffuser exit, are shown in figure 6. These data are for $M_0 = 1.8$, and similar results were obtained at $M_0 = 2.0$. For convenience in interpreting the data, the static pressure coefficients C_p at the points of measurement are also indicated. Static pressure fluctuations on the external cowl surface were measured at 45° from top center and 1.47 body diameters from the cowl lip. The dynamic pressure pickup with which this measurement was made was mounted in the center body and connected to the cowl surface with a 1/4-inch tube.

External and internal pressure fluctuations occurred initially at the same M_3 value and had identical frequencies. The amplitude

coefficients and the pressure amplitudes were, however, considerably less externally than internally. Considerably greater amplitudes and fluctuating pressure loads will undoubtedly be observed at external stations closer to the inlet lip. At 10° angle of attack, random external pressure pulsations of ± 3 pounds per square inch (ten times the maximum value at 0° angle of attack) were observed. 2254

The pulsation frequency could not be readily evaluated under burning conditions because combustion pulsations were superimposed on the diffuser pulsation, causing the pressure traces obtained to be quite irregular under supercritical as well as subcritical flow conditions. The combined effect of inserting the flame holder and burning was to dampen considerably the amplitude of the cold-flow subcritical diffuser pulse. At $M_3 = 0.145$, the amplitude coefficient of the diffuser-exit static pressure was reduced from a cold-flow value of 0.45 to a burning value below 0.04. This latter coefficient corresponds to a pressure variation of ± 0.72 pounds per square inch.

The damping influence exerted under burning conditions extended to the external pressure fluctuations as well. The above average amplitudes of the five conditions indicated on figure 6 are due to irregular random disturbances and not to subcritical diffuser instability.

Only the combined damping effectiveness of the flame holder and burning was obtained. The results obtained may therefore be peculiar to the burner configuration investigated and other configurations may amplify the pulse, causing combustor blow-out.

Typical pressure traces under subcritical and supercritical flow conditions are presented in figures 7 and 8, respectively. Subcritically, a regular pulsation was observed in the cold-flow case, whereas the combustion pulse was superimposed on this pattern in the burning case. Supercritically, low amplitude irregular pulses occurred during burning both at the diffuser exit and on the cowl surface. At a given M_3 the frequency and amplitude coefficient at the diffuser exit were approximately the same for both 0° and 6° angle of attack.

To indicate the normal shock travel for a typical subcritical operating condition, a sequence from a high-speed motion picture of the cold-flow shock movement at the cowl inlet for $M_0 = 2.0$, $\alpha = 6^{\circ}$, and a mass flow ratio m/m_0 of 0.784 is shown in figure 9.

Pressure distribution. - The longitudinal variation with mass flow and stream Mach number of the static pressure along the upper surface of the center body and the external static pressure along the top surface of the cowl are given for 0° angle of attack in figure 10(a). The pressure distributions on the internal surface of the cowl were essentially the same as those on the center body and therefore are not presented.

2254

The effect of mass flow ratio on the external cowl pressure coefficient beyond 0.8 body diameter from the lip was small and appears to be independent of stream Mach number. In the region between the lip and 0.8 body diameter, the values of C_p decrease as the mass flow ratio is reduced until at high spillage ratios C_p becomes negative and leading-edge suction occurs. The increase in C_p at 3 body diameters from the lip for $M_0 = 1.5$ was caused by reflection from the tunnel walls of the inlet shock disturbance.

Under supercritical flow conditions, a small contraction at the inlet caused an appreciable supersonic flow deceleration in the region between the cowl lip and 0.1 body diameter at $M_0 = 2$. The flow then reaccelerates until a normal shock occurs. Because the boundary layer cannot support an abrupt pressure rise, a branched shock configuration is indicated by the pressure coefficients. It would, therefore, be difficult to use a control mechanism designed to sense the normal shock position from static wall pressure. The irregularity in the pressure distributions from 1 to 1.5 body diameters at the maximum M_3 condition is thought to be due to the center-body support struts.

The effect of angle of attack and M_0 on the pressure distribution along the top and bottom surfaces of the cowl for critical inlet flow is shown in figure 10(b). At all three values of M_0, considerable lift resulted as the body was raised to positive angles of attack. At a given Mach number and angle of attack, the pressure coefficients on both top and bottom surfaces were essentially constant between 1.5 and 3.2 body diameters from the lip. Data were not taken beyond this latter position. Similar results have been obtained on bodies approximately half this size (reference 5).

The variation of the static pressures on the upper and lower surfaces of the center body with M_0 and angle of attack is shown in figure 10(c). On both surfaces, the angle of attack effects increase with M_0. The differences in pressure between the top and bottom surfaces are especially apparent at the lowest M_0 and occur in the region between the lip and 0.5 body diameter from the lip. At the higher values of M_0, some difference occurs in the region of the center-body support strut. The conclusion is reached that for angles of attack between 0° and 10°, internal forces normal to the engine axis are in general experienced in the region of the diffuser inlet.

Internal velocity distribution. - Representative data of the local Mach number variation at the air-flow measuring station, are shown in figure 11 for $M_0 = 1.8$. The same trends and essentially the same velocity profiles were noted under both cold-flow and burning conditions, figures 11(a) and 11(b). An essentially uniform circumferential velocity distribution resulted at 0° angle of attack. As the angle of attack was

increased, little effect on the flow was noted in the upper half of the annular duct but a shift in the peak velocities toward the center body was observed in the lower half of the duct. Similar results were obtained subcritically, except that the profiles in the upper half of the duct were somewhat flatter at angles of attack greater than 0° than the supercritical data shown. 2254

The effect of M_3 on the velocity distribution is demonstrated in figure 11(c). The peak velocities concentrate near the center body for subcritical flow and move toward the outer wall as the flow becomes supercritical. This same trend has also been observed with an engine of different design (reference 4).

Combustor performance. - Combustor performance with a constant-area outlet at $M_0 = 1.8$ is presented as typical of the effect of angle of attack on burner operation in figure 12. Increasing the angle of attack from 0° to 10° decreased the peak temperature ratio τ from 4.6 to 4.3, but did not noticeably change the other burner operating characteristics. This reduction is thought to be caused by the change in fuel-air distribution at the combustion chamber inlet. The operable fuel-air ratio range was limited by the fuel system rather than burner blow-out, and the burner was operated satisfactorily to 10° angle of attack from a value of M_3 as low as 0.18 to as high as 0.32 without instability or undue shell heating. With propylene oxide as fuel, ignition was obtained at 10° angle of attack as easily as at 0°, and for the configuration investigated no additional burner problems were introduced by operation at angles of attack to 10°.

Internal engine performance. - The typical effect of angle of attack on internal engine performance is shown in terms of the jet thrust coefficient for $M_0 = 1.8$, figure 13. The decrease in exit jet thrust at a given τ and M_0 as the angle of attack is increased results from two simultaneous effects, a reduction in diffuser pressure recovery and a drop in the mass air flow through the engine. In the M_0 range investigated, the reduction in jet thrust coefficient as the angle of attack was increased appeared independent of τ and was due primarily to the reduction in air flow.

The effect of angle of attack can be more readily interpreted if the net internal engine forces are presented in terms of the flight and lift directions. The horizontal (flight direction) net internal thrust coefficient C_H is based on a thrust value computed from the following equation

$$F_H = F_j \cos \alpha - m_a V_0$$

and the vertical (lift) component C_V based on a thrust computed from

$$F_V = F_j \sin \alpha$$

2254

The change in C_H and C_V with M_0, τ, and angle of attack is shown in figure 14. Although the specific data presented were obtained with the constant area exit nozzle, similar trends were observed with the other nozzle configurations investigated. By operating the engine at positive angles of attack, considerable lift can be derived from internal forces with only a small loss in F_H. For example, when the angle of attack was increased from 0° to 10°, reductions in C_H ranging from 7 to 15 percent occurred; however, at 10° angle of attack C_V values in the order of 30 to 50 percent of C_H were obtained. Thus, as a result of internal forces only, incremental lift to thrust ratios as great as 5 were attained.

At positive angles of attack, a sizeable lift is obtained not only from the vertical component of the internal engine forces but from the external aerodynamic forces on the engine body as well. Apart from stability considerations and changes in combustion efficiency, the desirability of flying a ram jet at positive angles of attack is determined by weighing the increase in body drag and the reduction in F_H against the lift achieved and the reduction in the required wing area which results. The analysis of reference 7 indicates that the range of a ram jet-powered vehicle may be increased by maintaining the engine at a positive angle of attack.

Effect of Exit Nozzle Configuration on Engine Performance

External body drag. - Body-drag coefficients for M_0 values from 1.5 to 2.0, given in reference 1 for the constant-area exit nozzle engine configuration, are reproduced in figure 15. The line of maximum mass flow ratio represents the minimum external body drag at each M_0, and the same minimum drag coefficient was observed under both cold-flow and burning conditions. The dashed line on figure 15 represents the minimum external drag of the converging exit-nozzle engine configuration and was obtained by adding the theoretical boattail drag to the minimum drag curve of the straight-pipe configuration. Because of the low boattail angle, identical values for boattail drags were computed from linearized theory and by the method of characteristics. The experimental minimum body drags under cold-flow conditions fell slightly below the theoretical values.

The supercritical external body drag with a conical converging exit nozzle, determined under burning conditions, indicates a considerable reduction in body drag over that obtained under cold-flow conditions, figure 16. The magnitude of this reduction increased with both M_0 and τ. At $M_0 = 2$ and $\tau = 3.6$, a reduction amounting to 45 percent of the supercritical cold-flow drag was observed.

Additional independent verification of this phenomenon could not be obtained with the limited measurements made. However, because the observed drag reduction exceeds the limitations of experimental accuracy it is thought that the converging nozzle actually is subject to increasing external pressures as the temperature of the jet is raised. A similar drag reduction has also been observed in wind tunnel tests of a small burning ram jet model (reference 8).

2254

Cold jets exhausting from a body with boattail and a relatively small amount of boundary layer have reduced the supersonic external body drag below that for the jet-off condition, (references 9 and 10). According to these data, the decrease in drag at pressure ratios similar to those of this investigation would be negligible. Yet it has been observed during this investigation and in others (references 11 and 12) that boattailed body drags with a hot jet are noticeably less than the jet-off or cold-jet condition. With burning, heat transfer through the wall of the combustion chamber can thicken the external boundary layer; but the fact that a change in drag did not occur with the constant-area exit negates the possibility of a friction drag effect. The phenomenon may be a tunnel-model interference effect. Other mechanisms which could also cause this drag reduction are discussed in reference 13.

Net internal thrust. - The effect of exit nozzle configuration on the net internal thrust coefficient C_t is shown in figure 17 as a function of M_3 for $M_0 = 1.5$, 1.8, and 2.0. The data for nozzle contraction ratios $\frac{A_6}{A_4}$ of 0.71 and 1.0 are based on tail-rake measurements, whereas the converging-diverging nozzle data were computed from balance measurements and an external body drag taken as equal to the cold flow drag of the $\frac{A_6}{A_4} = 1.0$ configuration. The theoretical net internal thrust of the converging-diverging outlet was determined by adding to the $\frac{A_6}{A_4} = 0.71$ data the thrust increment due to isentropic expansion in the diverging nozzle section. Since the experimental data fall above the theoretical curves, it is concluded that either the flow through the diverging section of the nozzle is not isentropic or the throat areas in the two cases are not identical. (A 2 percent difference in throat area could cause this apparent discrepancy.) In any case, at all M_0 values investigated the converging-diverging outlet gave a consistent and definite advantage over a conical converging outlet having the same geometric throat area.

The net internal thrust coefficients increase in both the subcritical and the supercritical regions as the value of M_3 is lowered by raising the total-temperature ratio τ. However, a break in the curve occurs at the critical flow condition. At a given M_3, maximum

2254

internal thrusts were obtained with the $\frac{A_6}{A_4} = 1.0$ configuration, because the engine was being operated at the highest τ value. Although the maximum experimental net internal thrust was obtained with the converging-diverging nozzle, $C_t = 0.85$ at $M_0 = 2.0$ and 0.84 at $M_0 = 1.8$, the widest net internal thrust coefficient range at all stream Mach numbers resulted for the $\frac{A_6}{A_4} = 1.0$ configuration.

Combustion efficiency. - The effect of the various exhaust nozzles on combustion chamber performance is shown in figure 18. Data are presented for 0° angle of attack and at a stream Mach number of 1.8 only, for in general these trends are typical of those obtained at the other angles of attack and M_0 values investigated. The fuel-air ratio range for each configuration is not significant, for there was no lean blow-out limit and the rich limit was again dependent on the maximum pumping capacity of the fuel system. (Stoichiometric fuel-air ratio for propylene oxide is 0.105.)

As expected, essentially similar combustor performance was observed for the converging and the converging-diverging nozzle configurations. The small difference in combustion efficiency which was observed is within the accuracy of the data. There is some evidence, however, that the flow through the diverging section is not isentropic, and if combustion is considered to occur in the diverging section, the difference between the two curves will be reduced.

Net engine performance. - In order to obtain a better comparison of nozzle configurations for range considerations, the external drags must also be considered. This can be done by presenting the reduced engine efficiency in terms of the propulsive thrust coefficient $(C_t - C_d)$, figure 19. The engine efficiency is basically the reciprocal of the thrust specific fuel consumption and has been reduced for convenience to 100 percent combustion efficiency to eliminate an additional variable. The values of M_3 and τ are also presented to aid analysis and interpretation of the data.

Over the range investigated, the results indicate that for a given propulsive thrust the $\frac{A_6}{A_4} = 0.71$ outlet is more efficient than the $\frac{A_6}{A_4} = 1.0$ outlet. (The $\frac{A_6}{A_4} = 1.0$ data were taken from reference 1.) Moreover, additional gain results if an internally expanding section is added at the nozzle outlet. At $M_0 = 2.0$, a maximum reduced engine efficiency of 21 percent and a maximum propulsive thrust coefficient of 0.68 were achieved. Progressively lower values resulted as M_0 was reduced.

Because there is some question concerning the true drag of the converging-nozzle configuration while burning, the cold-flow drag values were used in computing the data points plotted in figure 19. If the body drag determined under burning conditions is used instead, the gain resulting with the converging-diverging nozzle is slight. To show this effect, the variation of engine efficiency, based on burning drags, has also been included in figure 19.

When the total-temperature ratio is increased to the point where with a fixed geometry outlet the flow becomes subcritical, the total external body drag increases and the diffuser total-pressure recovery generally falls. Although this combination of circumstances permits continued increases in the propulsive thrust, it ultimately results in a reduction in the engine efficiency. Such a trend is apparent for the $\frac{A_6}{A_4} = 0.71$ configuration at $M_0 = 1.8$ and 1.5 where, although (C_t-C_d) continued to increase with τ, the rising fuel-consumption rate caused a reduction in engine efficiency.

The engine is potentially capable of greater propulsive thrusts with a constant-area nozzle than with a contracted outlet. If the (C_t-C_d) data is plotted as a function of M_3 for the several nozzle configurations investigated, (fig. 20), the magnitude of the propulsive thrust differences is more readily apparent. The greater propulsive thrusts developed with the uncontracted outlet is due to the higher τ values required to maintain a given inlet flow condition.

Durability of Graphite Nozzle

In many suggested ram jet designs, graphite has been proposed as a desirable exit nozzle material. However, little information is available on the use and durability of graphite for such applications. The engine was initially operated with a graphite nozzle for about 20 minutes at $M_0 = 1.8$, 2.0, and 0° angle of attack. The engine was then run for approximately 30 minutes at $M_0 = 2.0$, 6° and 10° angles of attack, and $M_0 = 1.6$, 0° angle of attack (data not presented). During these runs the engine was operated over a range of fuel flows and the graphite nozzle was subjected to temperatures sufficiently high to cause it to glow.

Inspection of the graphite insert indicated no appreciable surface wear or deterioration. Temperature-sensitive paints indicated that the outer surface of the shell in a region on top center and ahead of the graphite nozzle insert had reached 1100° F, but that no part of the shell surrounding the insert had reached this temperature. The method of retaining the graphite nozzle insert in the outer shell proved satisfactory and caused no difficulty in fabrication.

SUMMARY OF RESULTS

The following results were obtained from an investigation of a 16-inch ram jet engine in the NACA Lewis laboratory 8- by 6-foot supersonic tunnel. Data were obtained with three exit nozzle configurations at angles of attack from 0° to 10° and Mach numbers from 1.5 to 2.0.

1. For the burner configuration used, a change in engine angle of attack from 0° to 10° caused a reduction in combustion efficiency of about 10 percentage points with no reduction in range of operation or ease of ignition.

2. Some losses in diffuser total-pressure recovery and maximum mass flow occurred as the angle of attack was changed from 0° to 10°. The magnitude of these losses increased with stream Mach number and angle of attack. Similar velocity distributions at the diffuser exit and the same diffuser performance were obtained under cold-flow and burning conditions.

3. A considerable lift can be achieved from internal forces by operating the engine at positive angles of attack with only small losses in horizontal thrust.

4. Subcritical pressure fluctuations at the diffuser exit amounting to as much as ± 7.4 pounds per square inch were observed under cold-flow conditions. These fluctuations were damped out in the burning case, the greatest amplitude observed being about ± 0.7 pounds per square inch. Little change in amplitude was observed in the cold-flow case when the angle of attack was increased from 0° to 6°, but the change from 6° to 10° caused a considerable reduction in amplitude.

5. As predicted by theory the cold-flow engine body drag increased slightly when the constant-area exit nozzle was replaced with a converging nozzle. There is some evidence, however, that the engine body drag with a boat-tailed afterbody may be appreciably less under burning than cold-flow conditions.

6. Maximum engine efficiencies were obtained with a converging-diverging exit nozzle configuration.

7. A graphite converging-diverging exit nozzle was operated for a period of 50 minutes at temperatures sufficiently high to cause the graphite to glow. The durability of the insert proved satisfactory and no cracking or erosion occurred during this period of operation.

Lewis Flight Propulsion Laboratory
National Advisory Committee for Aeronautics
Cleveland, Ohio

REFERENCES

1. Nussdorfer, T., Wilcox, F., and Perchonok, E.: Investigation at Zero Angle of Attack of a 16-Inch Ram-Jet Engine in 8- by 6-Foot Supersonic Wind Tunnel. NACA RM E50L04, 1950.

2. Perchonok, Eugene, Wilcox, Fred A., and Sterbentz, William H.: Preliminary Development and Performance Investigation of a 20-Inch Steady-Flow Ram Jet. NACA ACR E6D05, 1946.

3. Perchonok, Eugene, Sterbentz, William H., and Wilcox, Fred A.: Performance of a 20-Inch Steady-Flow Ram Jet at High Altitudes and Ram-Pressure Ratios. NACA RM E6L06, 1947.

4. Perchonok, Eugene, and Farley, John M.: Internal-Flow and Burning Characteristics of 16-Inch Ram Jet Operating in a Free Jet at Mach Numbers of 1.35 and 1.73. NACA RM E51C16, 1951.

5. Esenwein, Fred T., and Valerino, Alfred S.: Force and Pressure Characteristics for a Series of Nose Inlets at Mach Numbers from 1.59 to 1.99. I - Conical Spike All-External Compression Inlet with Subsonic Cowl Lip. NACA RM E50J26, 1951.

6. Sterbentz, William H., and Evvard, John C.: Criterions for Prediction and Control of Ram-Jet Flow Pulsations. NACA RM E51C27, 1951.

7. Howard, E., Luidens, R. W., and Allen, J. L.: Force and Pressure Characteristics for a Series of Nose Inlets at Mach Numbers from 1.59 to 1.99. V - Analysis and Comparison on Basis of Ram-Jet Aircraft Range and Operational Characteristics. NACA RM E51G23

8. Singham, J. R., Pruden, F. W., and Tomlinson, R. C.: Tests on a Working Model Ram Jet in a Supersonic Wind Tunnel. Rep. No. R-20, British N.G.T.E., Nov. 1947.

9. Erdmann: Widerstandsbeiwerte für das A4V1P mit Berücksichtigung des Strahl - und Reibungseinflusses für Unter- und Überschallgeschwindigkeiten-Untersuchung der Strahlexpansion. Peenemunde Archiv No. 66/105, Märs 24, 1943. (Trans. H. P. Liepmann, Goodyear Aircraft Corporation, R-30-18, Part 19, Feb. 15, 1946.)

10. Love, Eugene S.: Aerodynamic Investigation of a Parabolic Body of Revolution at Mach Numbers of 1.92 and Some Effects of an Annular Jet Exhausting from the Base. NACA RM L9K09, 1950.

2254

11. Stoney, William E., Jr., and Katz, Ellis: Pressure Measurements on a Sharply Converging Fuselage Afterbody with Jet On and Off at Mach Numbers from 0.8 to 1.6. NACA RM L50F06, 1950.

12. Edson, J. B.: Optical Studies of the Jet Flame of the V-2 Missile in Flight. Rep. 708, Ballistic Res. Labs. (Aberdeen Proving Ground, Md.), Oct. 1949.

13. Hebrank, W. H., and Hicks, B. L.: A Preliminary Study of the External Ram Jet. Memo. Rep. No. 522, Ballistic Res. Labs. (Aberdeen Proving Ground, Md.), Oct. 12, 1950. (Project No. TB3-0110 of the Res. and Dev. Div., Ord Corps.)

2254

2254

TABLE I - 16-INCH RAM-JET COORDINATES

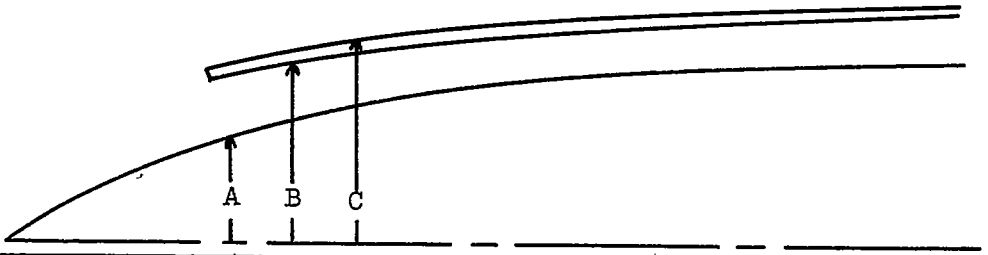

Station (in.)	Location	A (in.)	B (in.)	C (in.)
-5.05	Tip of spike	0		
-4.0	(cone half-angle 25°)	0.48		
-3.0		0.94		
-2.0		1.41		
-1.0		1.88		
0	Lip of inlet	2.34	5.05	
1.0	(radius 0.032 in.)	2.78	5.13	5.37
2.0		3.10	5.30	5.54
3.0		3.36	5.45	5.69
4.0		3.58	5.59	5.83
6.0		3.94	5.83	6.07
8.0		4.21	6.03	6.28
10.0		4.40	6.20	6.45
12.0		4.52	6.36	6.61
14.0		4.58	6.48	6.72
16.0		4.60	6.58	6.82
18.0	Station 2	4.58	6.61	6.85
30.0		4.44	Straight	Straight
46.0		4.02	taper	taper
59.0	Station x	3.08	7.75	8.13
63.0		2.43	7.45	Cylindrical
68.4	End of center body	0	7.38	section
81	Pilot air inlets	1.5		
93	Pilot maximum diameter	4.0		
107	Station 3	3.3	8.00	
169	Exhaust nozzle inlet		8.00	8.13
187	Nozzle exit			

NACA

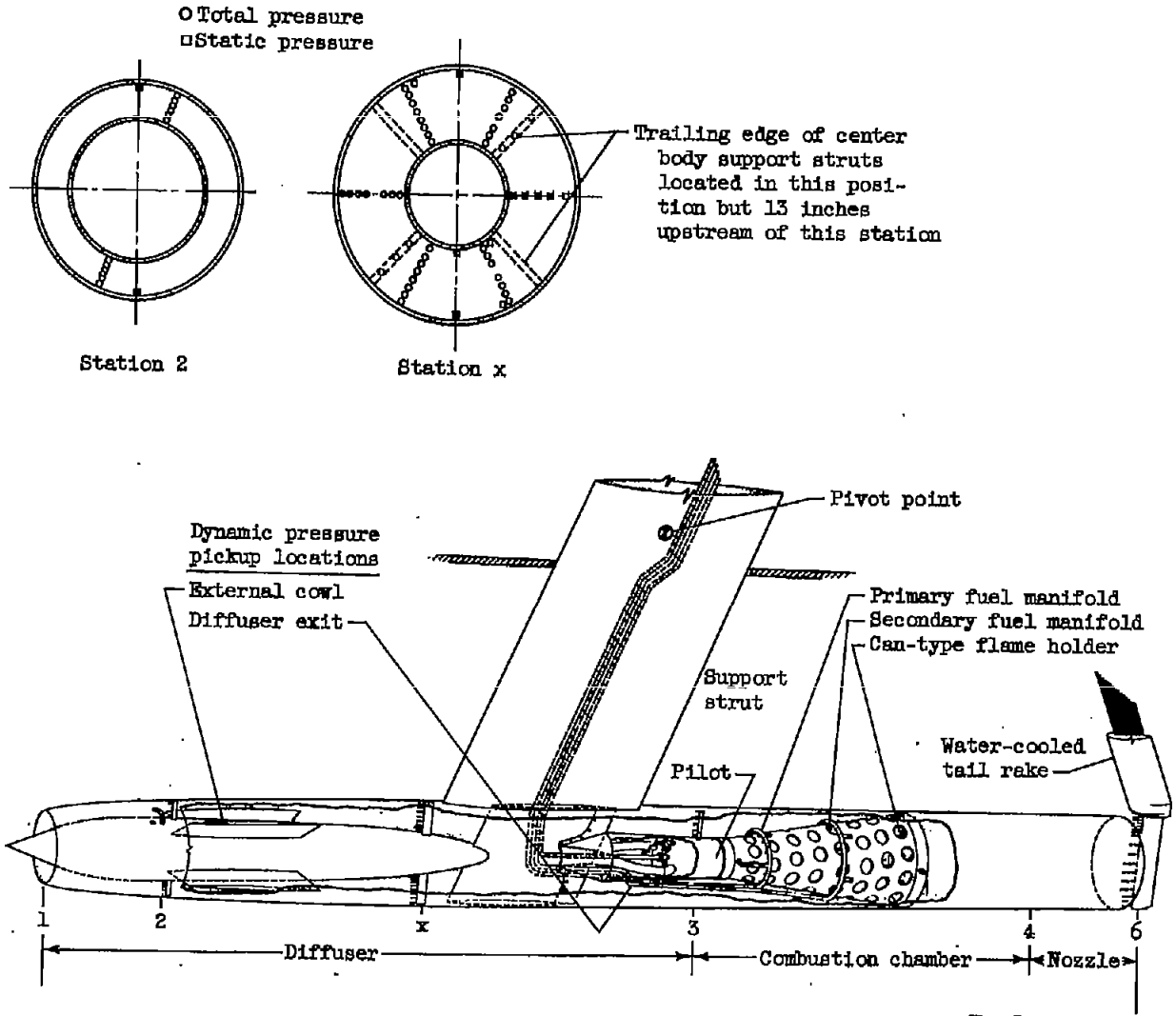

Figure 1. - Diagrammatic sketch of 16-inch ram jet.

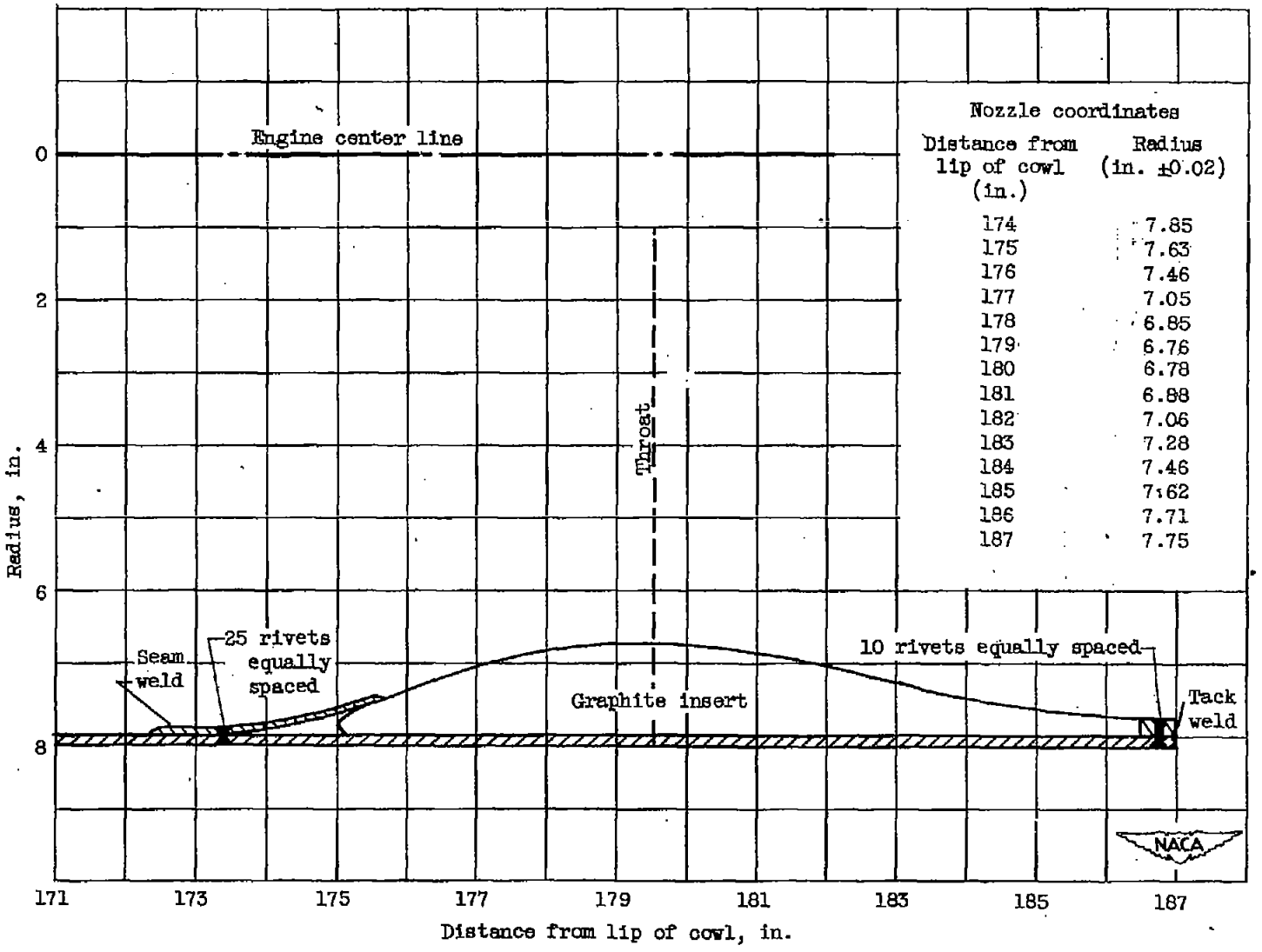

Nozzle coordinates

Distance from lip of cowl (in.)	Radius (in. ±0.02)
174	7.85
175	7.63
176	7.46
177	7.05
178	6.85
179	6.76
180	6.78
181	6.88
182	7.06
183	7.28
184	7.46
185	7.62
186	7.71
187	7.75

Figure 2. - Converging-diverging exhaust-nozzle coordinates and mounting details.

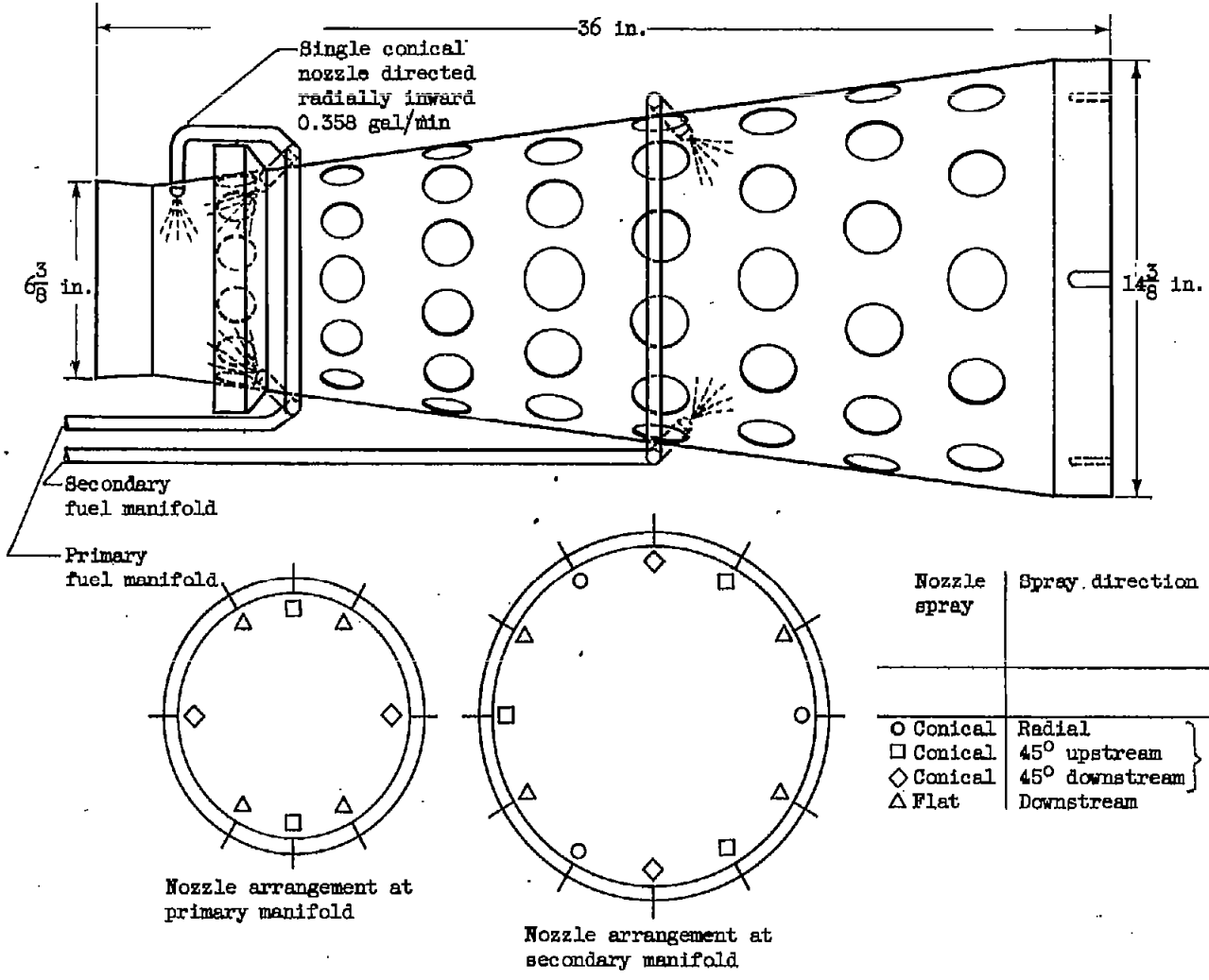

Nozzle spray	Spray direction	Nozzle rating (at 100 lb/sq in.) (gal/min)	
		Primary manifold	Secondary manifold
○ Conical	Radial		
□ Conical	45° upstream	0.667	1.000
◇ Conical	45° downstream		
△ Flat	Downstream	.625	.625

Figure 3. - Burner-configuration details.

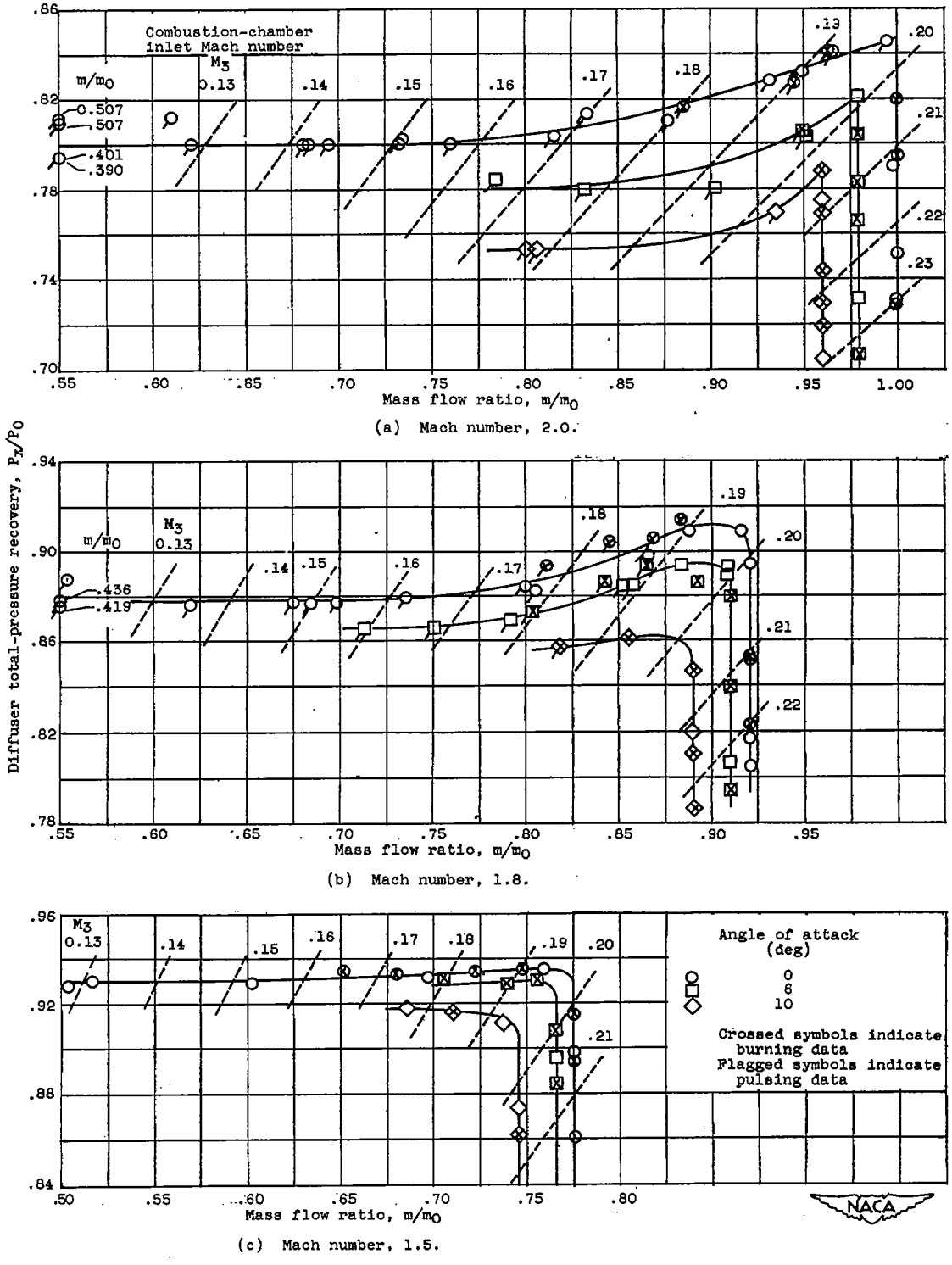

(a) Mach number, 2.0.

(b) Mach number, 1.8.

(c) Mach number, 1.5.

Figure 4. - Diffuser performance at Mach numbers 1.5, 1.8, and 2.0 for angles of attack of 0°, 6°, and 10°.

2254

2254

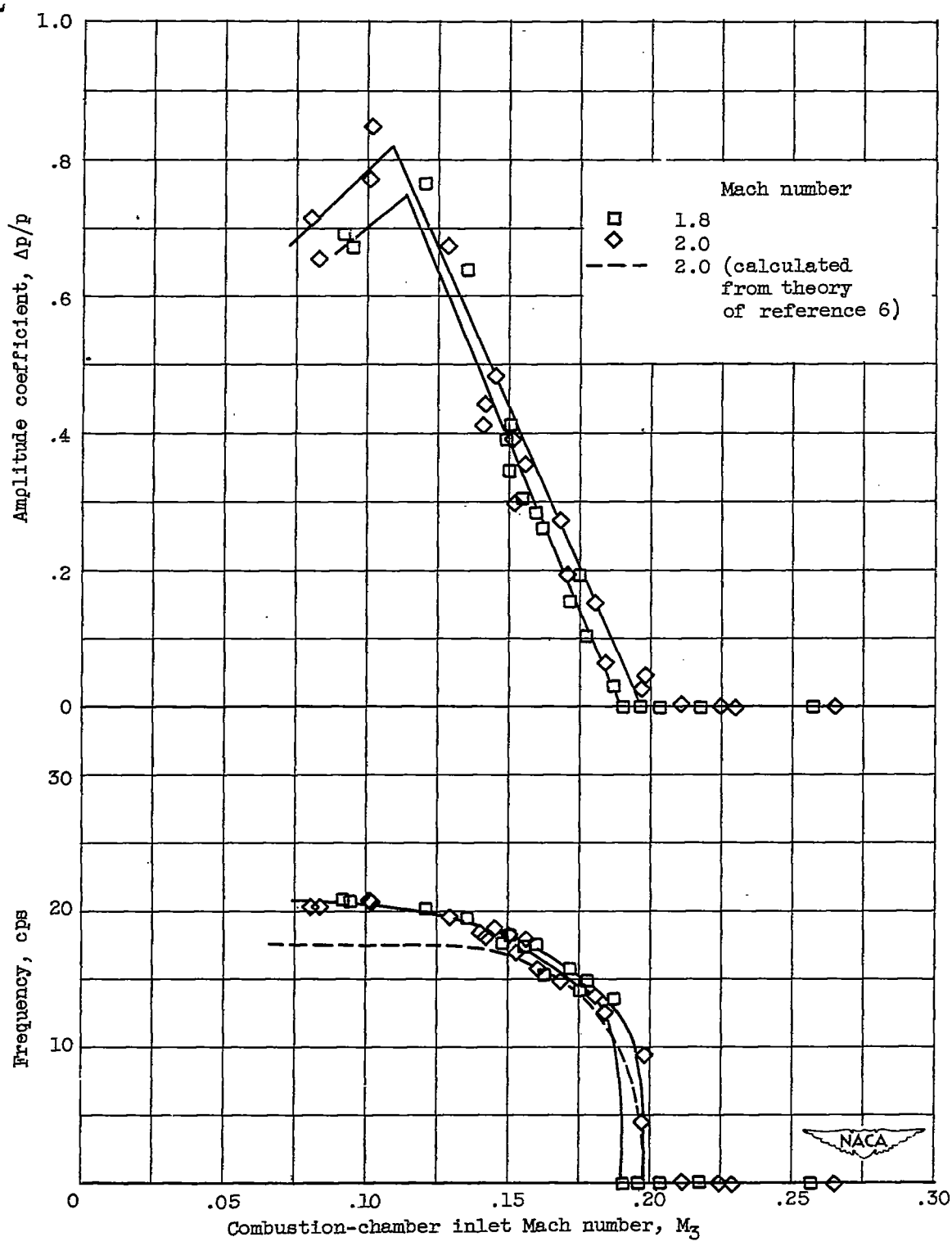

Figure 5. - Cold-flow static pressure fluctuation at diffuser exit; 0° angle of attack.

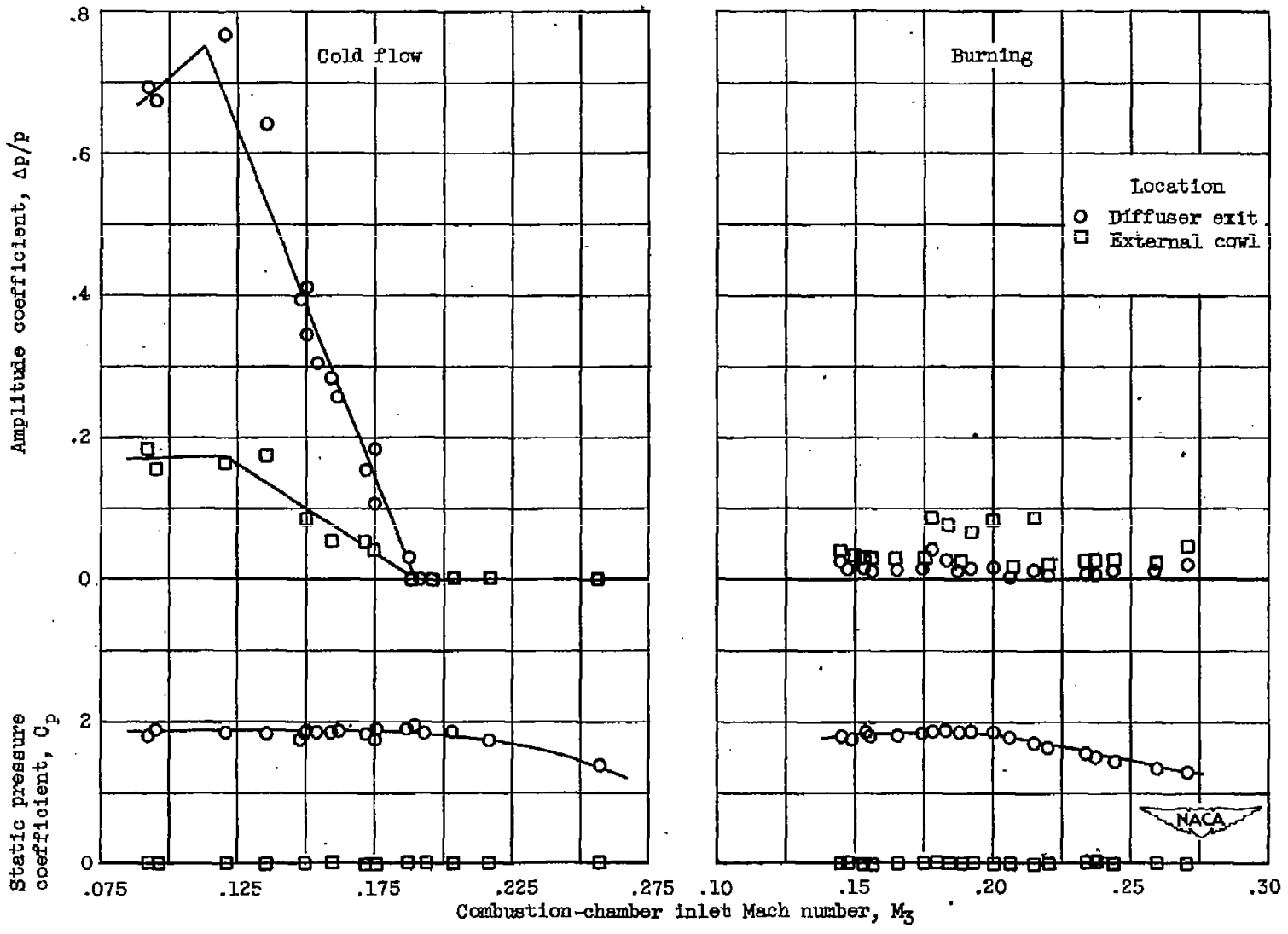

Figure 6. - Static-pressure fluctuation at diffuser exit and external surface of cowl for cold-flow and and burning conditions. Mach number, 1.8; angle of attack, 0°.

2254

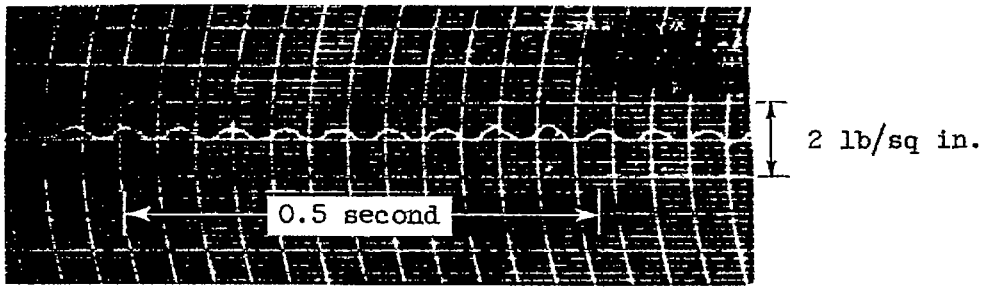

External cowl

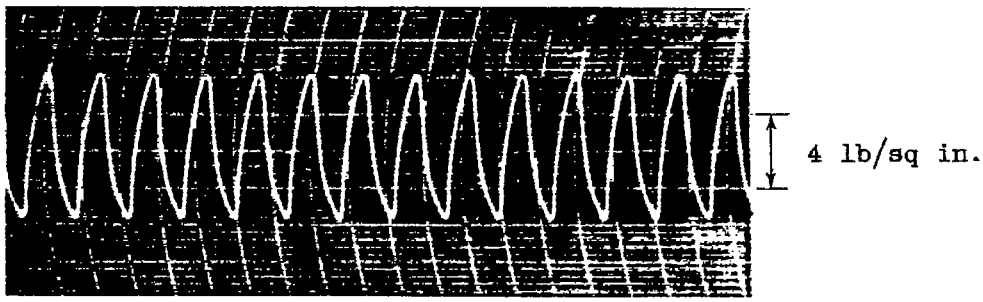

Diffuser exit

(a) Cold, combustion-chamber inlet Mach number, 0.150.

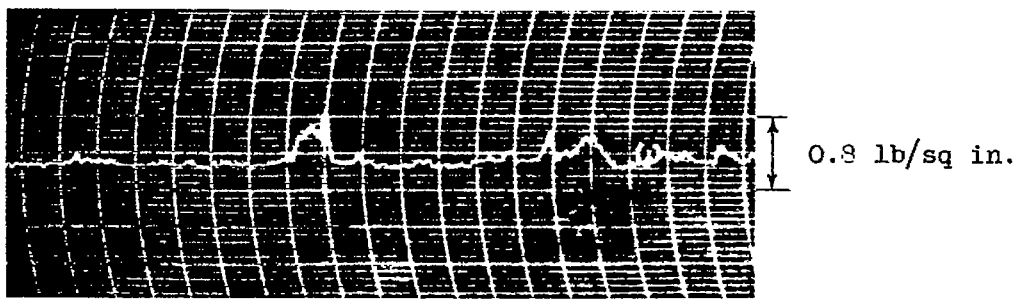

External cowl

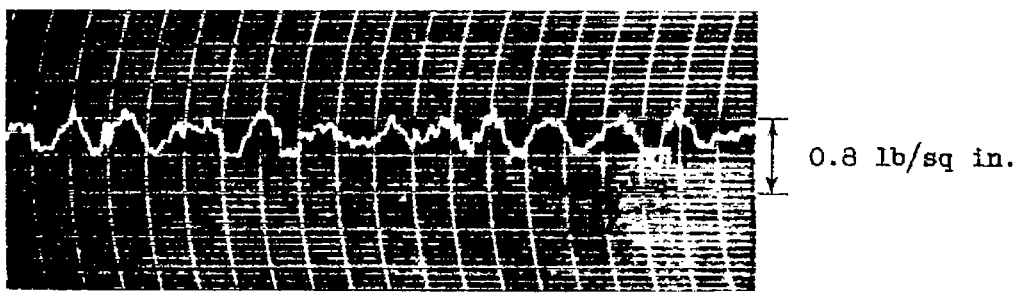

Diffuser exit

(b) Burning, combustion-chamber inlet Mach number, 0.153.

Figure 7. - Effect of burning on diffuser pressure pulsations. Free-stream Mach number, 1.8; constant-area exhaust nozzle.

[redacted]

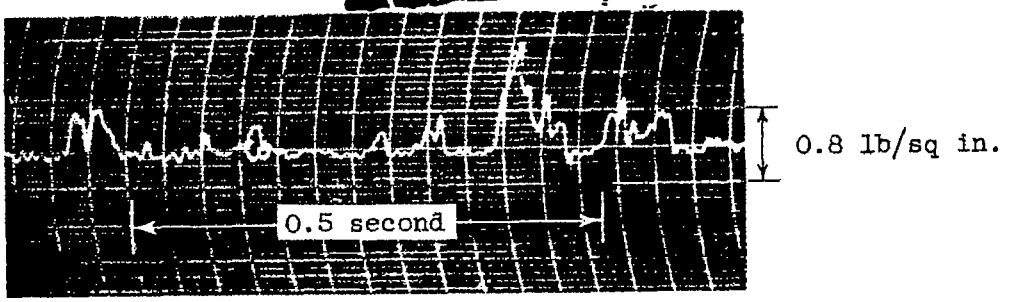

External cowl

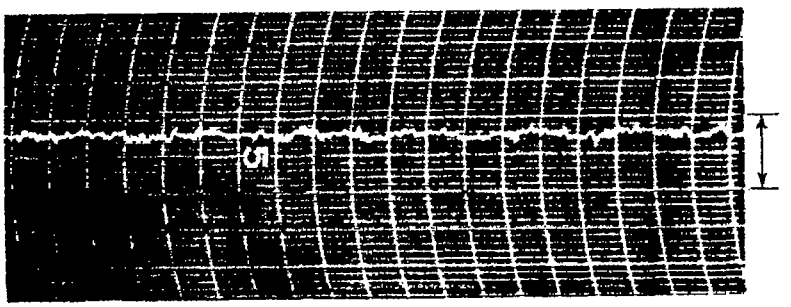

Diffuser exit

(a) Combustion-chamber inlet Mach number, 0.259.

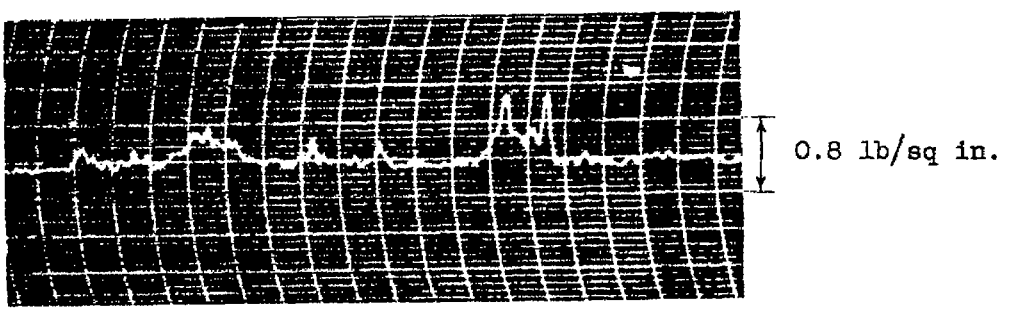

External cowl

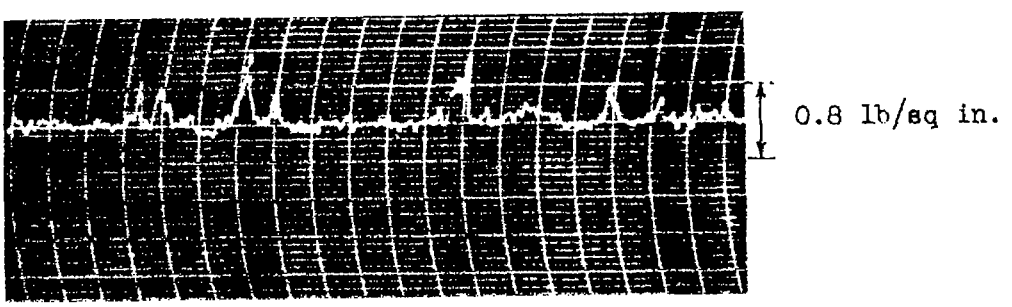

Diffuser exit

(b) Combustion-chamber inlet Mach number, 0.200.

Figure 8. - Internal and external diffuser pressure pulsations with burning for supercritical operation. Free-stream Mach number, 1.8.

2254

2254

(a) Beginning of cycle.

(b) 12.5 percent of cycle.

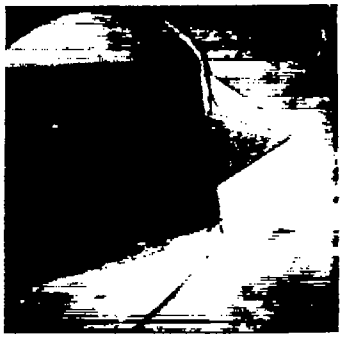

(2) 25 percent of cycle.

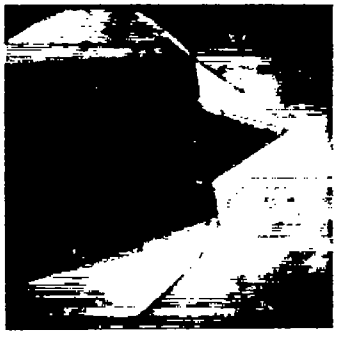

(d) 37.5 percent of cycle.

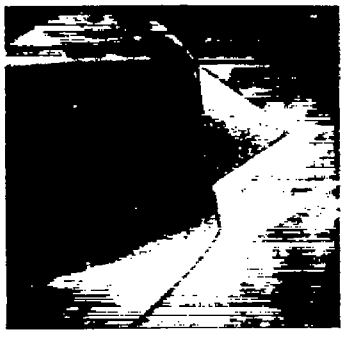

(e) 50 percent of cycle.

(f) 62.5 percent of cycle.

(g) 75 percent of cycle.

(h) 87.5 percent of cycle.

(i) End of cycle.

NACA
C-28106

Figure 9. - Sequence of photographs at inlet for cold-flow operation at Mach number 2.0 taken by high speed motion picture camera. Angle of attack, 6°; frequency, 18.7 cycles per second; diffuser exit amplitude coefficient, 0.36; combustion-chamber inlet Mach number, 0.165.

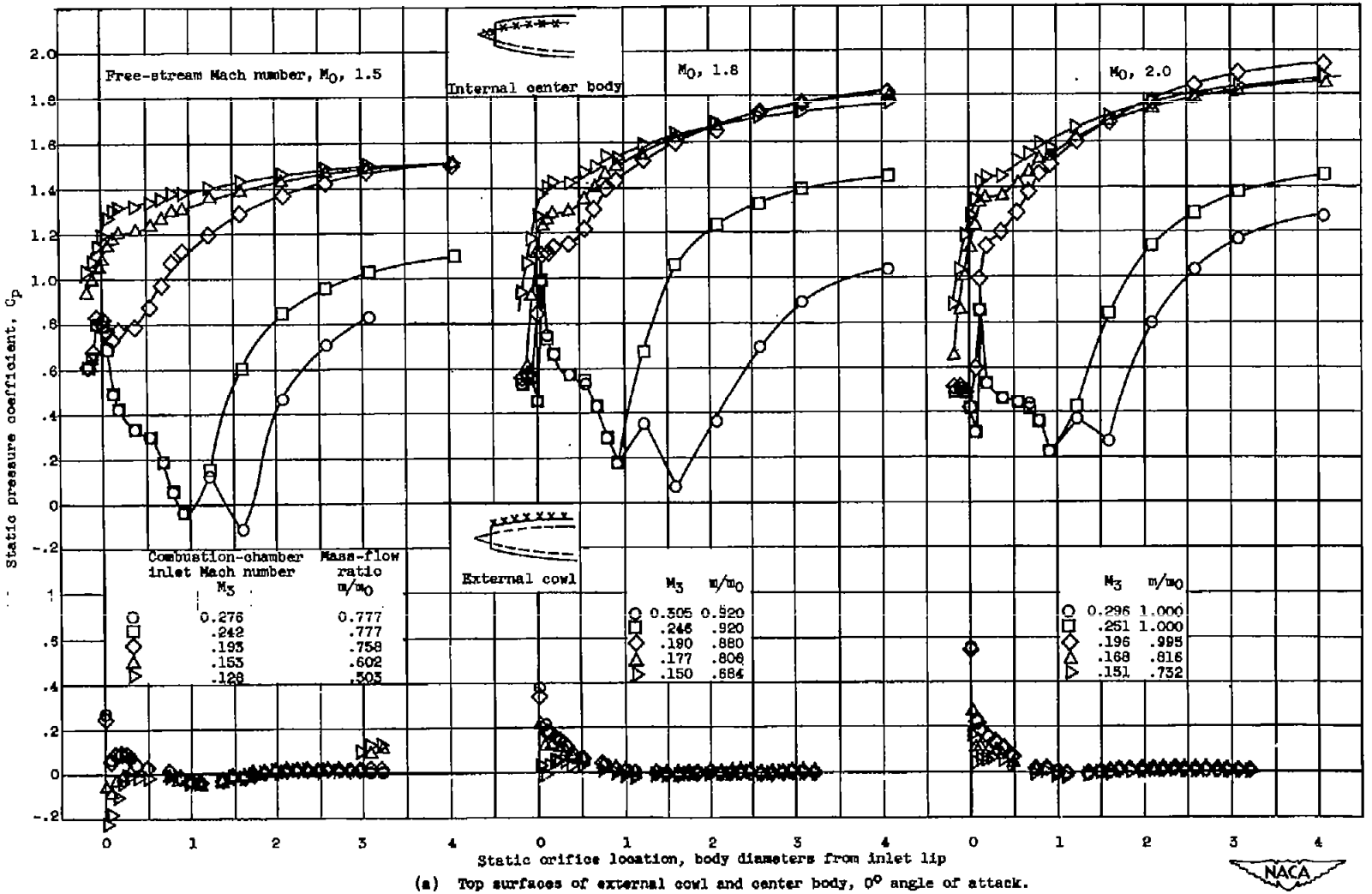

(a) Top surfaces of external cowl and center body, 0° angle of attack.

Figure 10. - Variation in static pressure coefficients along diffuser at free-stream Mach numbers of 1.5, 1.8, and 2.0.

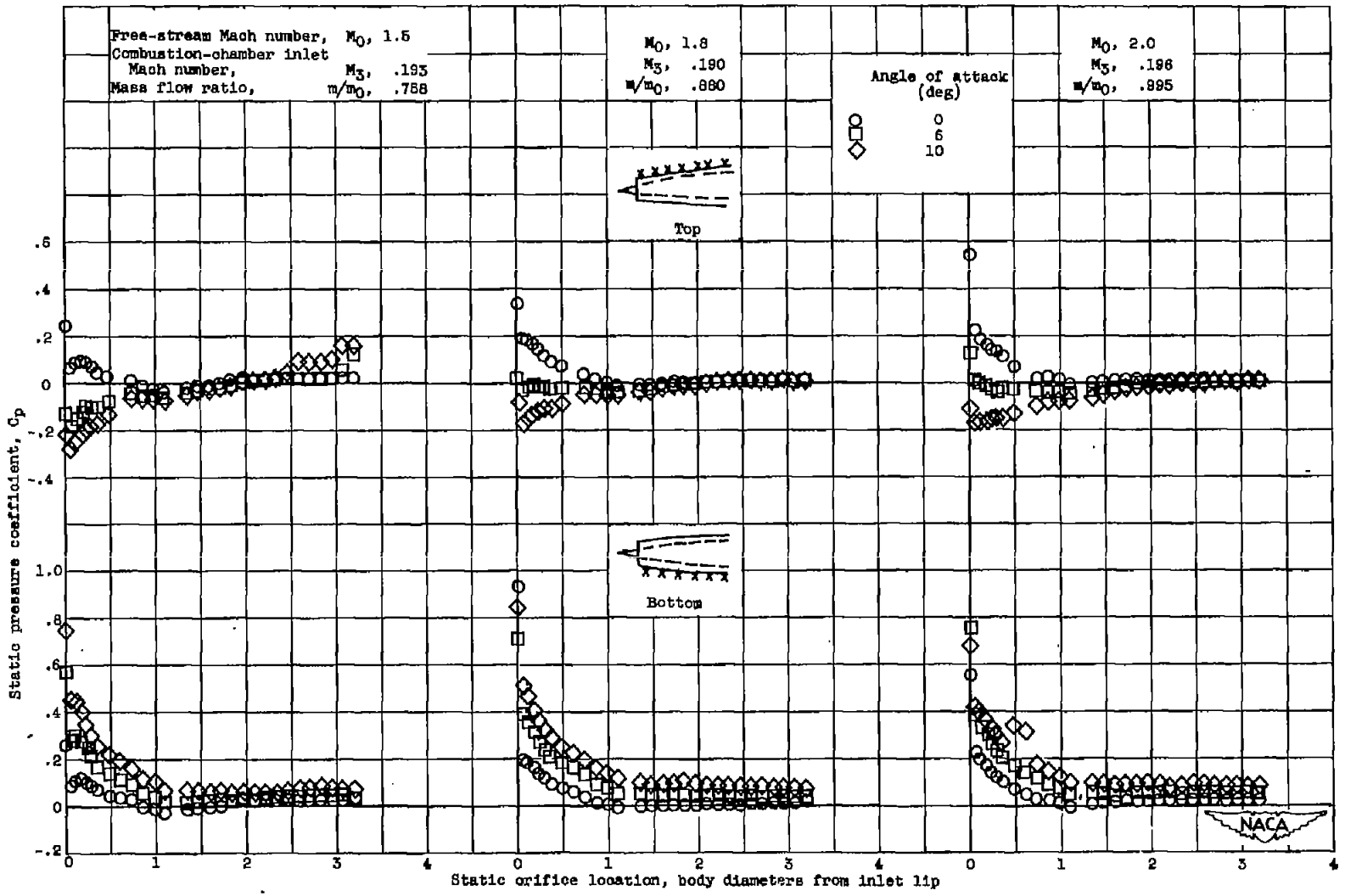

(b) Top and bottom external cowl surfaces at angles of attack of 0°, 6°, and 10°.

Figure 10. - Continued. Variation in static pressure coefficients along diffuser at free-stream Mach numbers of 1.5, 1.8, and 2.0.

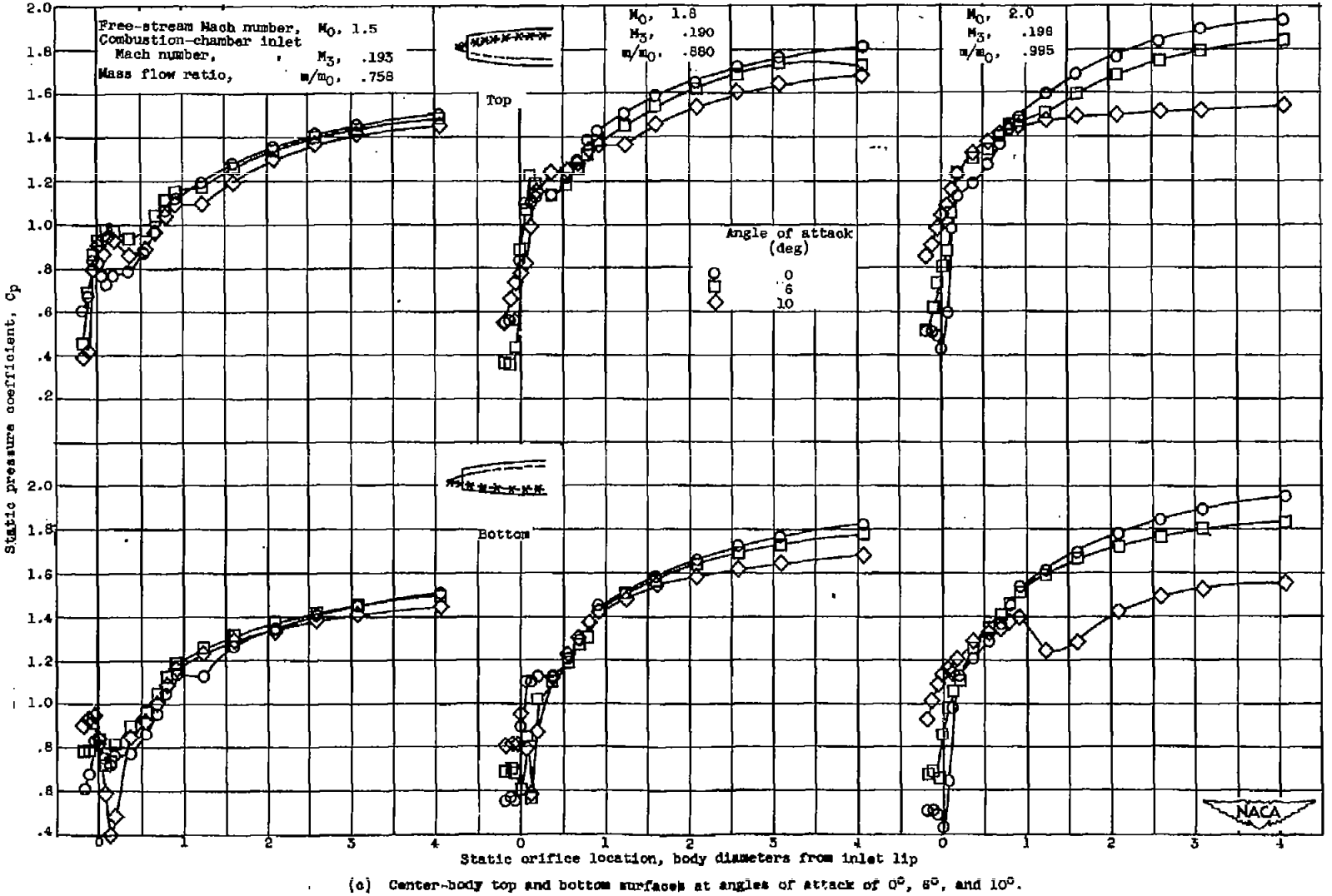

(c) Center-body top and bottom surfaces at angles of attack of 0°, 6°, and 10°.

Figure 10. - Concluded. Variation in static pressure coefficients along diffuser at free-stream Mach numbers of 1.5, 1.8, and 2.0.

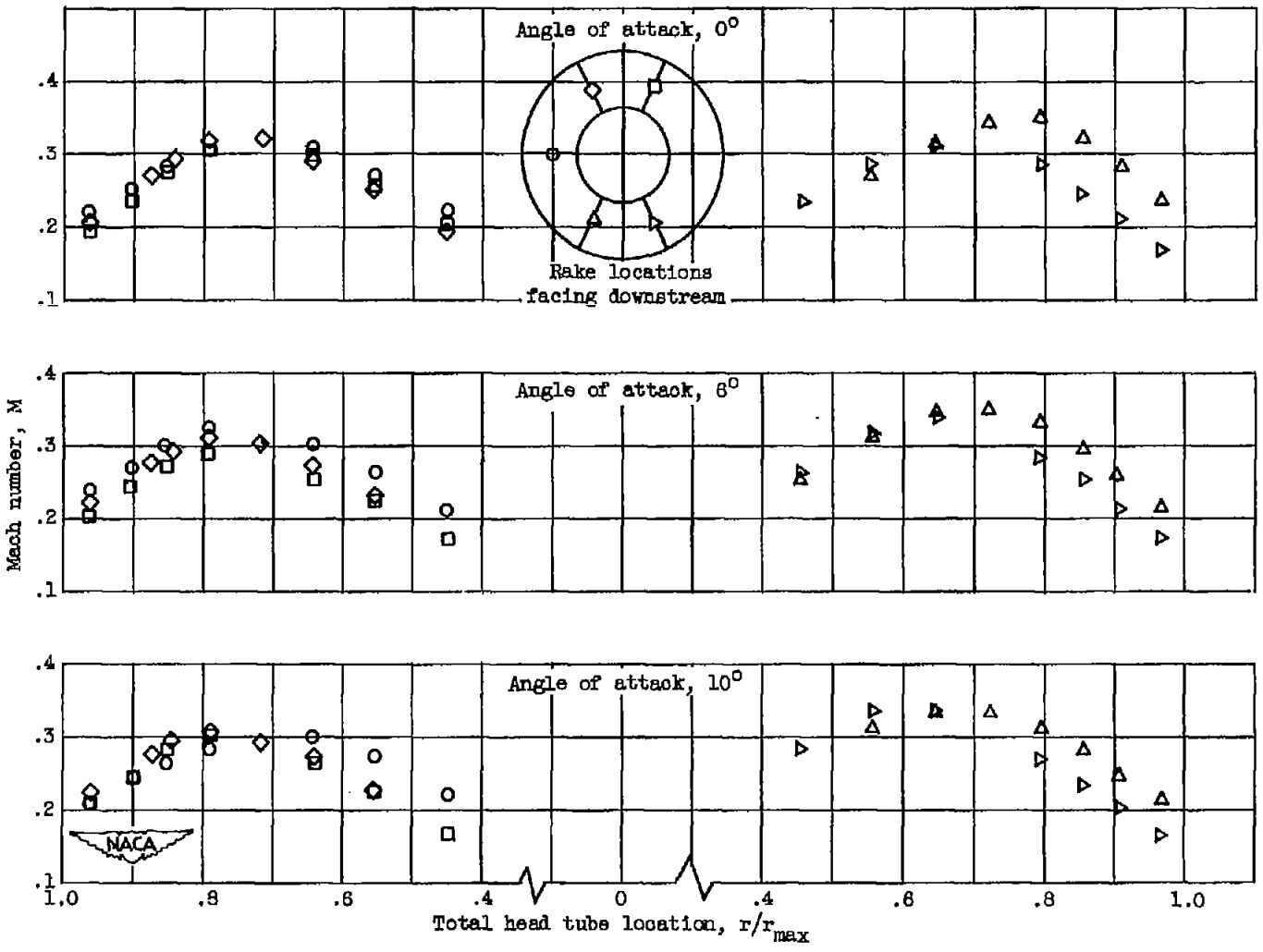

(a) Effect of angle of attack; cold flow; combustion-chamber inlet Mach number, 0.22.

Figure 11. - Profiles of Mach number distribution at station x; free-stream Mach number, 1.8.

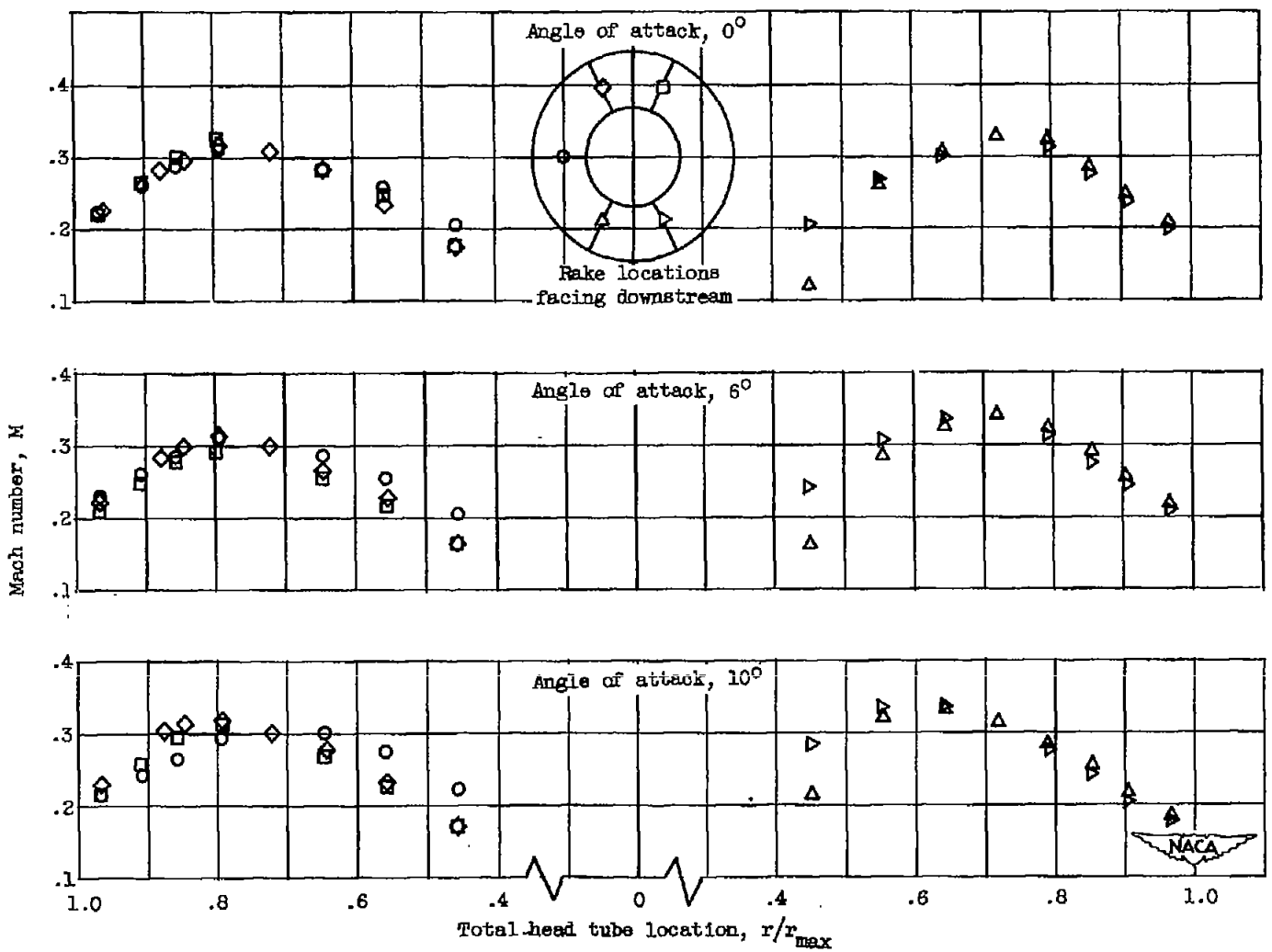

(b) Effect of angle of attack; burning; combustion-chamber inlet Mach number, 0.22.

Figure 11 - Continued. Profiles of Mach number distribution at station x; free-stream Mach number, 1.8.

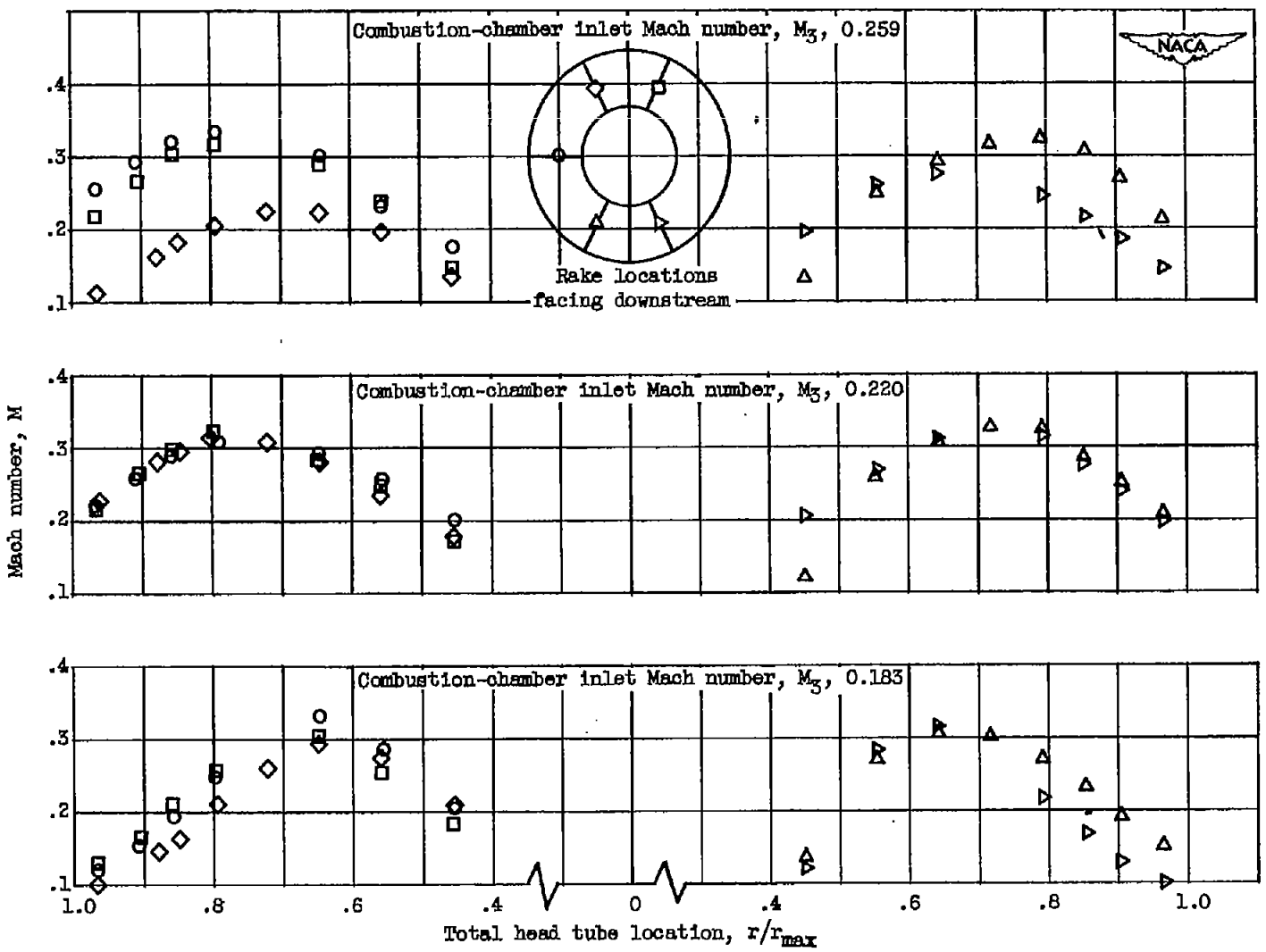

(c) Effect of combustion-chamber inlet Mach number, M_3; burning; angle of attack, 0°.

Figure 11. - Concluded. Profiles of Mach number distribution at station x; free-stream Mach number, 1.8.

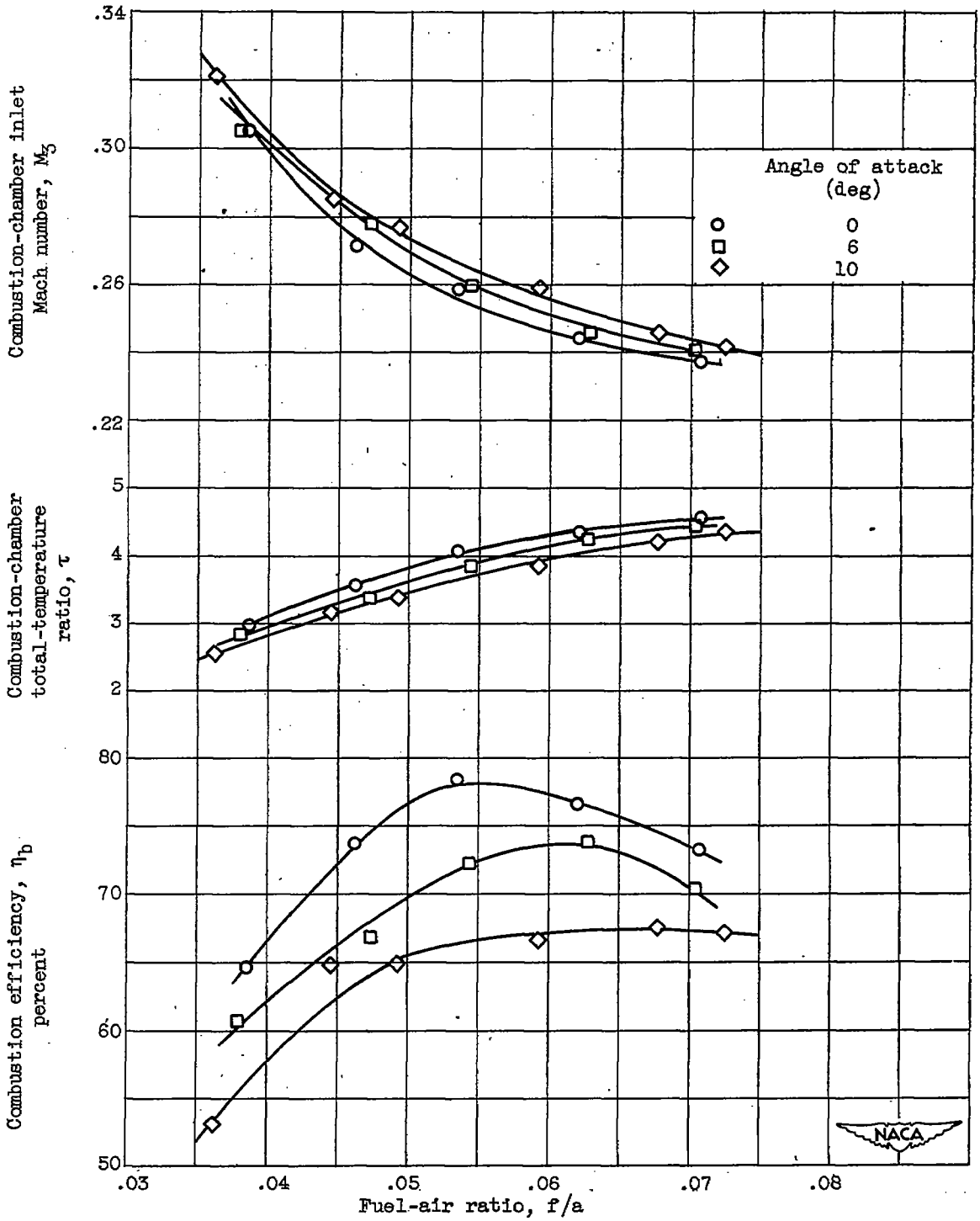

Figure 12. - Effect of operation at angle of attack on combustion. Mach number, 1.8; constant-area outlet nozzle; combustion-chamber inlet temperature, 135° F; static pressure, 1700 to 2200 pounds per square foot abolute.

2254

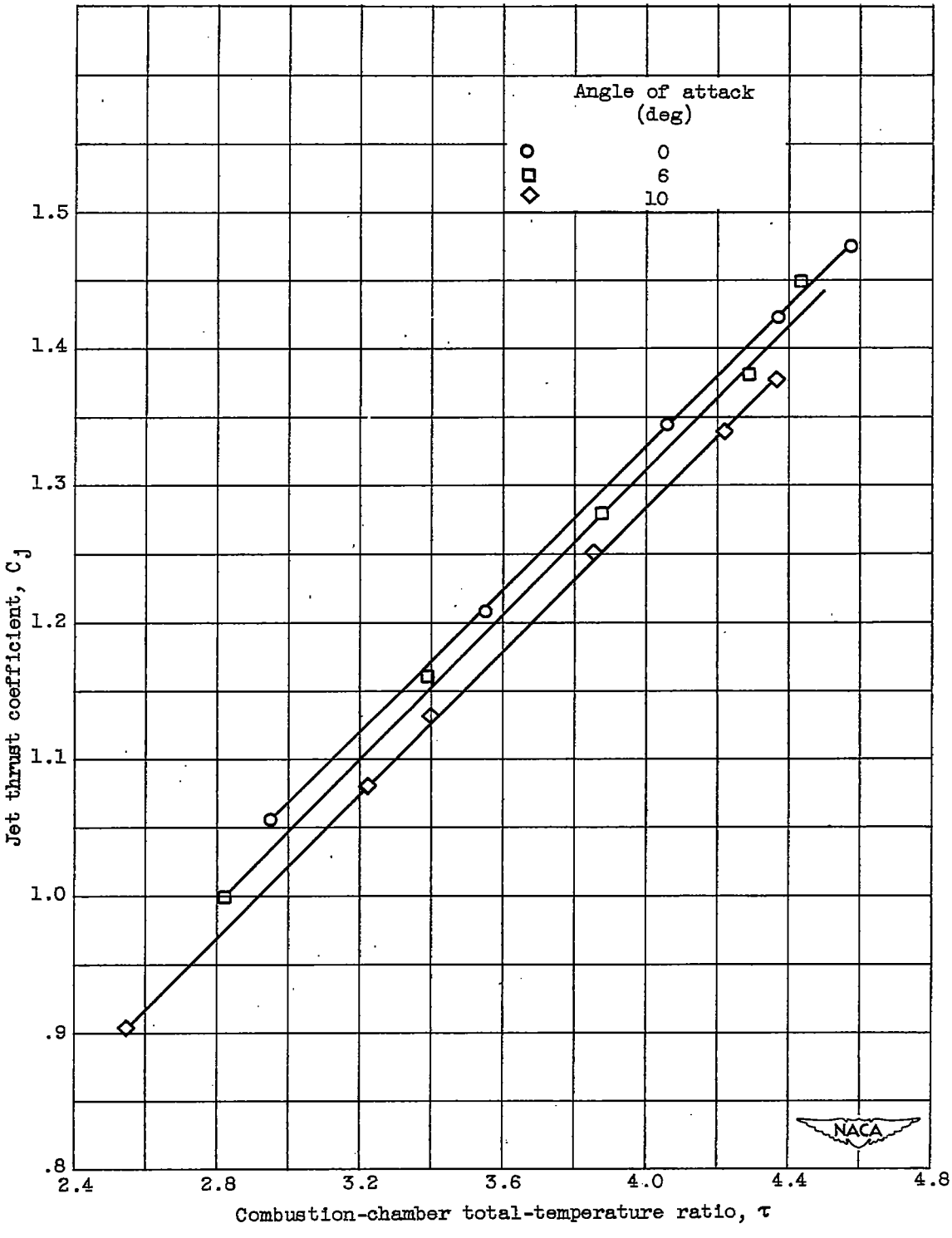

Figure 13. - Jet thrust coefficients obtained with constant-area outlet nozzle at Mach number of 1.8 and angles of attack of 0°, 6°, and 10°.

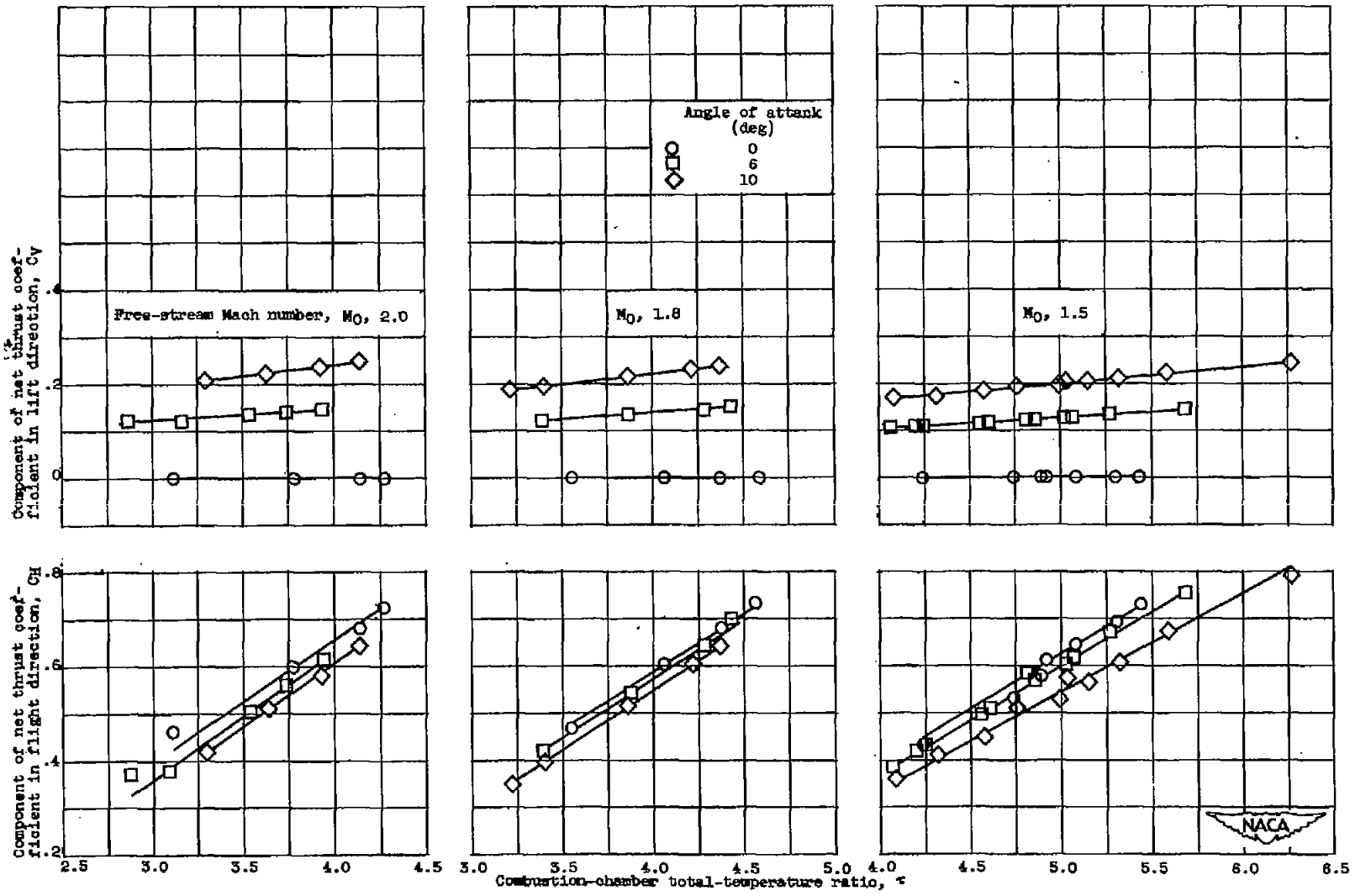

Figure 14. - Components of net thrust coefficients in flight and lift directions at angles of attack of 0°, 6°, and 10° at Mach numbers 1.5, 1.8, and 2.0 for constant-area exhaust nozzle.

2254

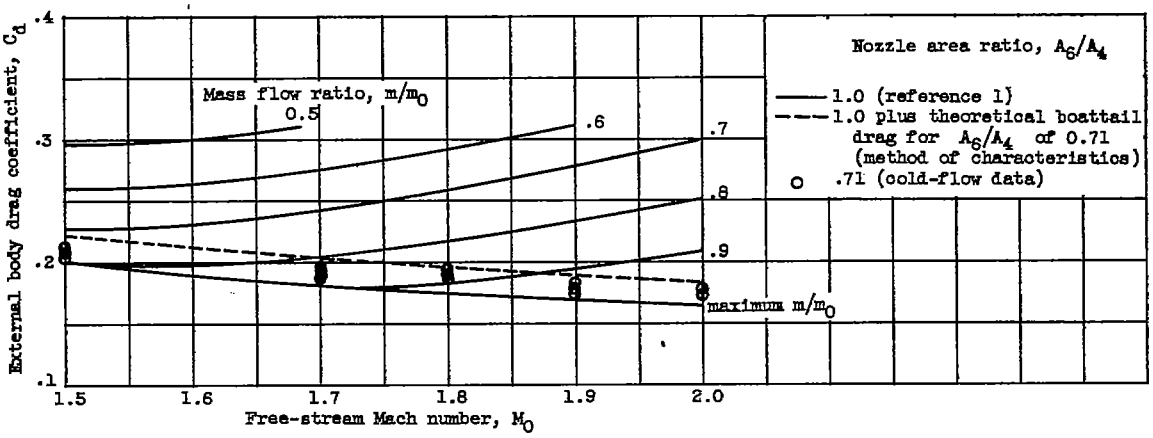

Figure 15. - Cold-flow engine body drag coefficients for 16-inch ram jet with constant area and converging exhaust nozzles.

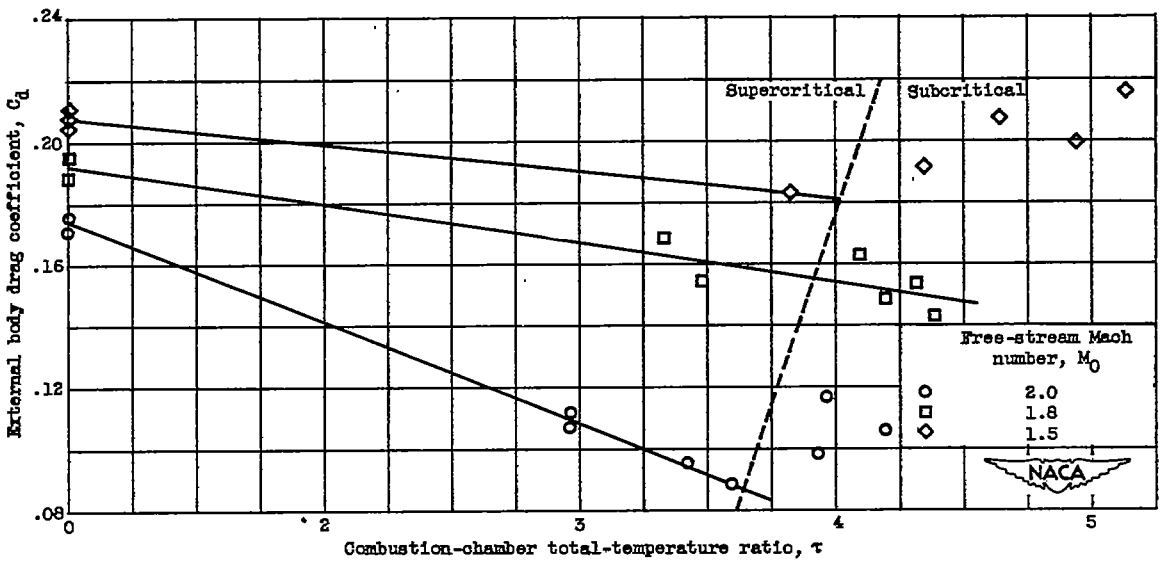

Figure 16. - Effect of burning on body drag coefficient for converging outlet nozzle at free-stream Mach numbers of 1.5, 1.8, and 2.0 and 0° angle of attack.

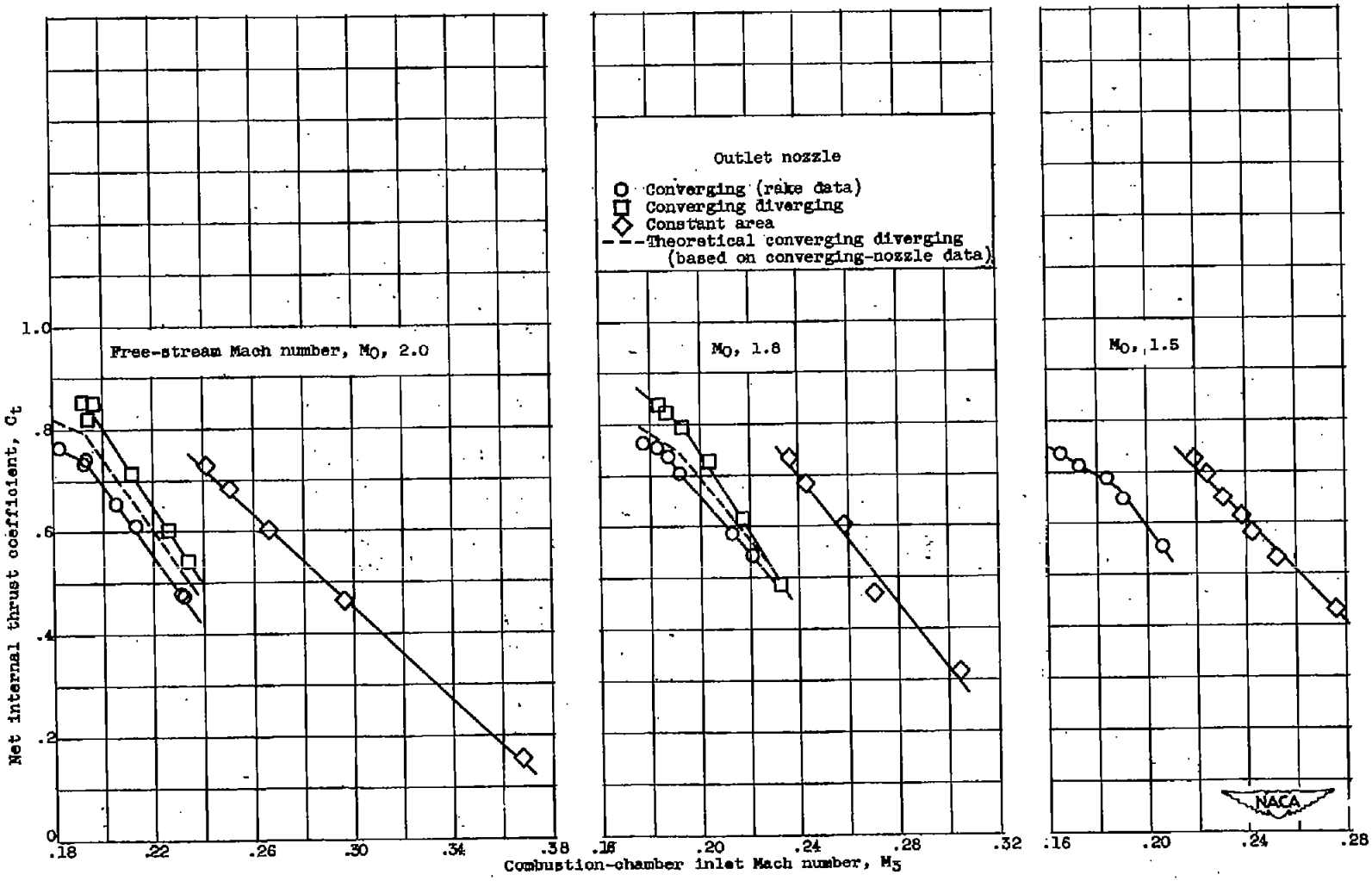

Figure 17. - Net internal thrust coefficients obtained with the three outlet nozzles at Mach numbers of 1.5, 1.8, and 2.0 at 0° angle of attack.

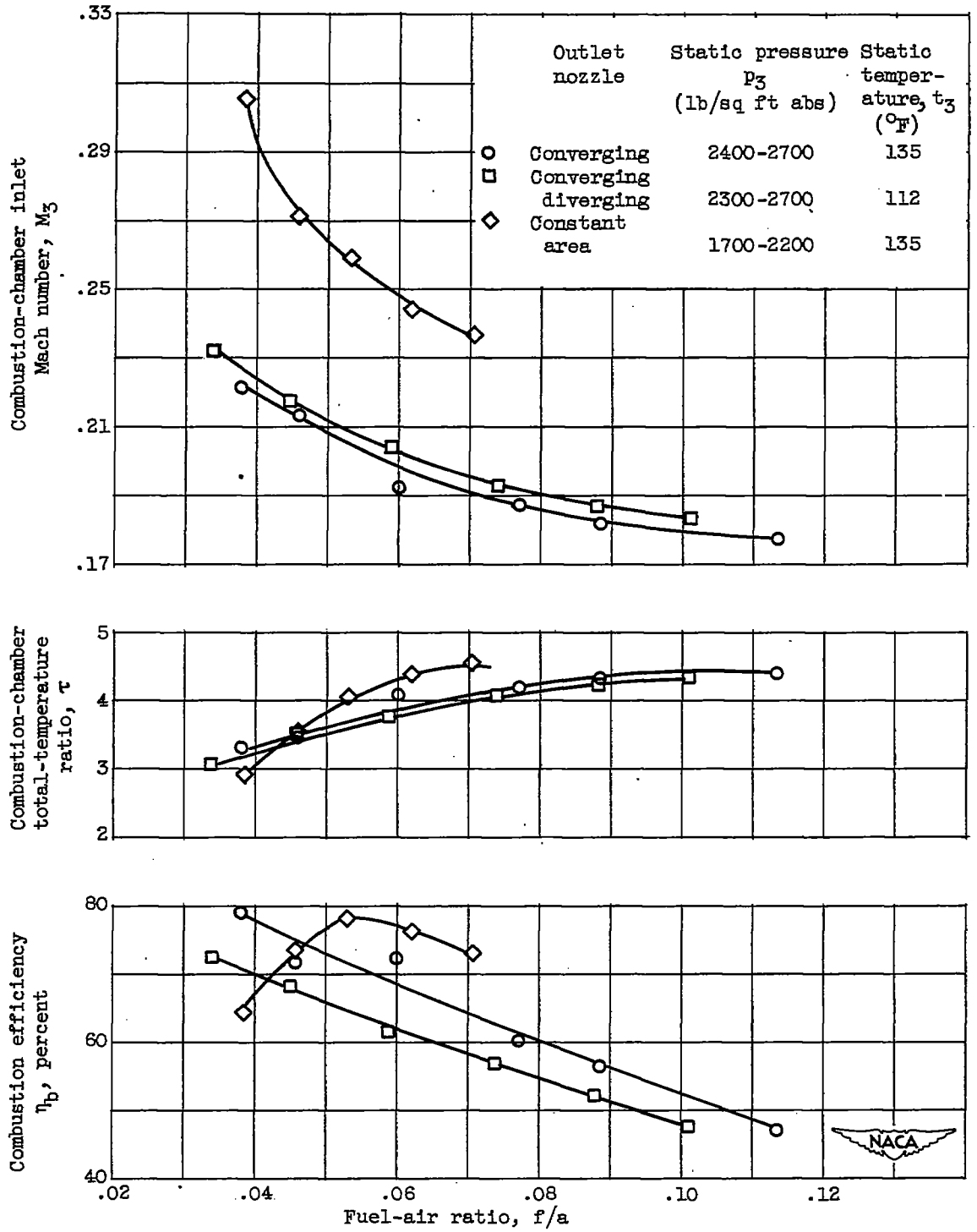

Figure 18. - Effect of outlet nozzle configuration on combustor performance at free-stream Mach number of 1.8 and 0° angle of attack.

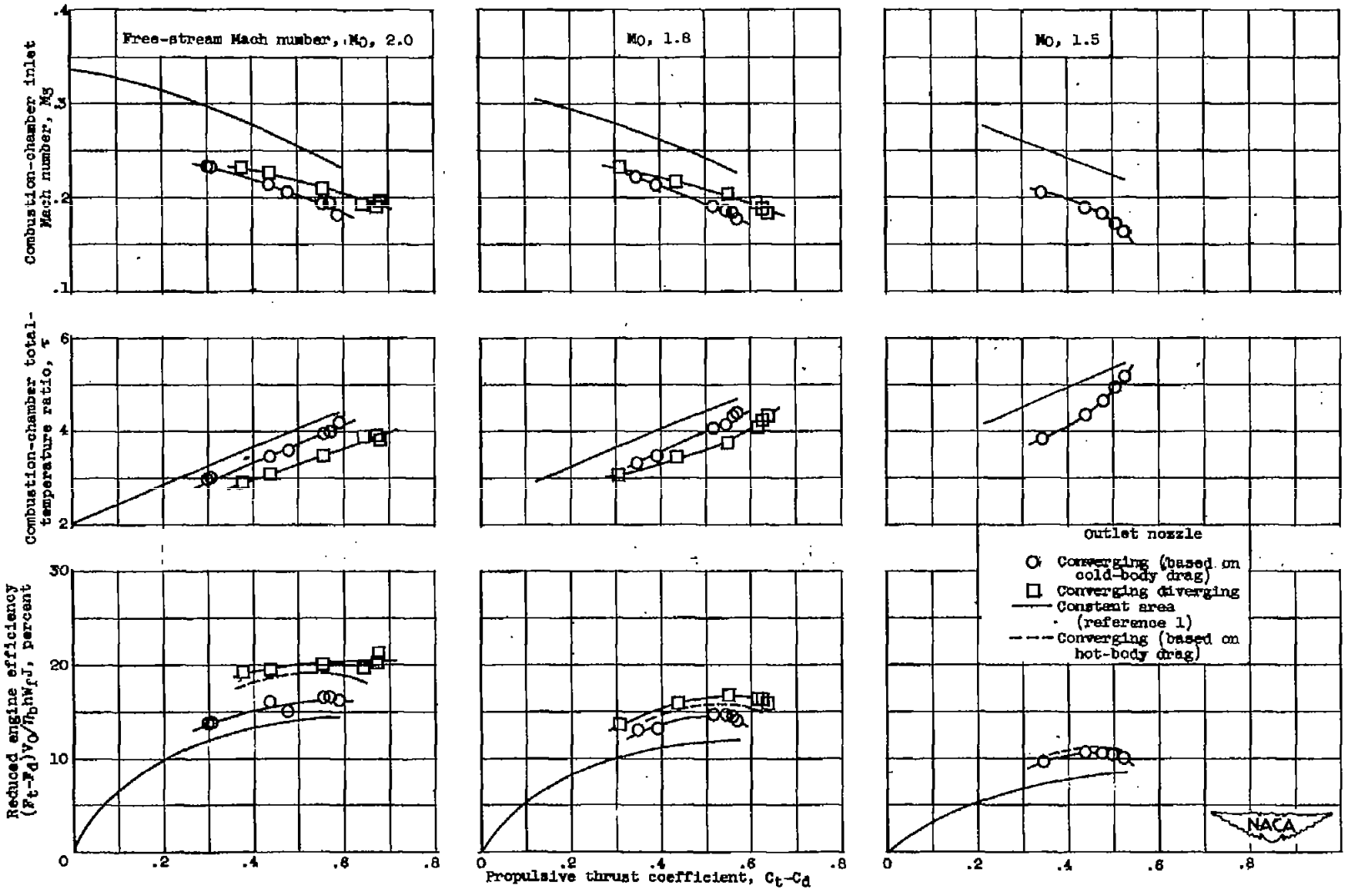

Figure 19. - Variation of reduced engine efficiency with propulsive thrust coefficient for the three outlet nozzles at Mach numbers of 1.5, 1.8, and 2.0 and 0° angle of attack.

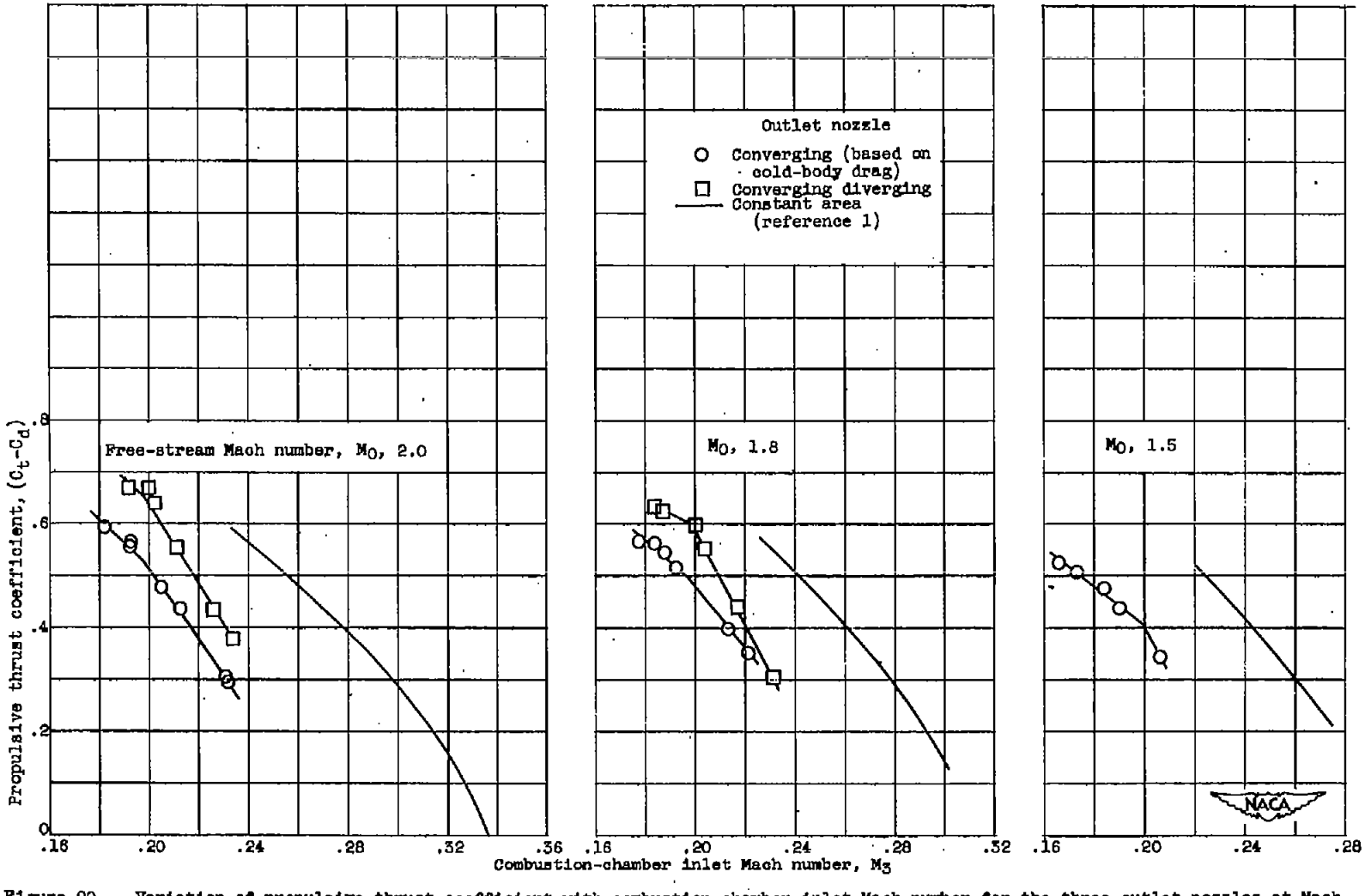

Figure 20. - Variation of propulsive thrust coefficient with combustion-chamber inlet Mach number for the three outlet nozzles at Mach numbers of 1.5, 1.8, and 2.0 and 0° angle of attack.

NACA-Langley - 10-5-51 - 500